Copyright© owned by the author of this thesis. Permission is given for a copy to be downloaded by an individual for the purposes of research and private study only. The thesis may not be reproduced elsewhere without the permission of the author.

Wavelet Signal Processing of Human Muscle Electromyography Signals

By

Amur Hamed Mohammed Almanji

A thesis in partial fulfilment of the requirement for the degree of

Masters of Engineering

In

Mechatronics

Massey University

Albany

New Zealand

2010

Abstract

A novel tool of biosignal processing is proposed to identify human muscle action through sEMG. The tool is based on the integration of continuous wavelet transforms, the Wavelet time entropy and the Wavelet frequency entropy to identify muscle actions through sEMG. The experiments are carried out on triceps, biceps and flexor digitorum superficialis (FDS) muscles. sEMG signals are measured at different intensities of FDS muscle contractions in order to verify the consistency of results. By taking the average entropies and basing it on the lowest average wavelet entropy, it was found in calibrated experiments that the complex Shannon wavelet family is the best candidate to identify the muscle activities among: derivative of Gaussians wavelet family, derivative of complex Gaussians wavelet family, complex Morlet family, Symlets, Coiflets and Daubechies wavelet families. Moreover, the results are consistent with the time-variant signal. The results presented in this paper have futuristic engineering implications in biomedical engineering and bio-robotic applications.

The proposed method has the potential of development, improvement and extension to include other wavelets. Future work includes compromising two wavelets that have different properties on both time and frequency domains, such as the complex Shannon wavelet (with very good frequency resolution but a slow decay in the time domain) and the Meyer wavelet (with good frequency resolution but a faster decay than the complex Shannon wavelet in the time domain), in order to produce optimal results of Wavelet time entropy and Wavelet frequency entropy.

Preface

This report is a result of my Master's Thesis project conducted at Massey University, Albany Campus.

I wish to express my gratitude to my supervisor Dr Jen-Yuan Chang (James); without his unlimited support and valuable guidance this thesis would not have been possible.

It is a pleasure to thank Dr Carlo Liang for his valuable explanations of the mathematical aspects in my research, Dr Steven Brown for his unique assistance in neuromuscular systems, Simon Bennets for his help in the laboratory setup and data measurements.

Finally, I would like to thank Maha Osman, all my friends and family members for their unlimited support. Their support, both direct and indirect, gave me confidence during times of difficulty.

I hope this report will guide knowledge seekers to further development in the world. I would like to conclude my preface with the following proverb:

A drop of knowledge is greater than an ocean of strength.

Table of Contents

Abbreviations

CWT: Continuous Wavelet Transform

DOCG: Derivative of Complex Gaussian

DOG: Derivative of Gaussian

EMD: Empirical Mode Decomposition

EMG: Electromyography

FDS: Flexor Digitorum Superficial

GT: Gabor Transform

HHT: Hilbert Huang Transform

IMF: Intrinsic Mode Function

sEMG: Surface Electromyography

SNR: Signal Noise Ratio

STFT: Short Time Fourier Transform

TF: Time-Frequency

TFA: Time-Frequency Analysis

WFE: Wavelet Frequency Entropy

WT: Wavelet Transform

WTE: Wavelet Time Entropy

WFB: Wavelet Filter Bank

WVD: Wigner-Ville Distribution

List of Figures

List of Tables

Chapter 1: Introduction

1.1 Project Overview

Machine–human interaction, based on features of human biological signals, is one of the key focuses and has drawn significant research attention in the field of medical robotics. The integration of biosignals with machine components and embedded control algorithm to form intelligent mechatronics devices is expected to assist with human daily activities and to provide services to humans when working in hazardous environments. Typical examples of medical robotics and bio-mechatronic devices are surgical assistant systems, medical imaging devices and exoskeleton robots (Jiang, Parker, & Englehart, 2007). In recent years, mind control technology based on brain signals and power has obtained a popular reputation around the world. Moreover, it will be one of the main expansions in the human-machine interaction field.

The rapid development of bio-robotics is a result of people's constant need to overcome present problem, like amputation, and inventing bio-mechtronics devices to mimic how human parts function. This trend has been under focus since the last century, where researchers have been integrating their knowledge in different areas such as medicine, engineering, physiology, etc. (Hof, 1984). In this thesis, an integration of signal processing (engineering) and biomedical aspects have been integrated to discover and travel through the world of biomedical engineering.

As reported in Castellini, Fiorilla, & Sandini (2009) and Winter (2009), Electromyography (EMG)-based control is one of the potential researches around the world. EMG signals are electrical signals produced by the activation of the muscle's motor units. These signals are non-stationary (Ismail & Asfour, 1998; Rafiee, Schoen, Prause, Urfer, & Rafiee, 2009). They are normally a function of time, commonly analyzed in terms of the signal's amplitude, frequency content and phase information relative to the reference signal.

Existing techniques used to measure EMG signals include surface methods and intramuscular or indwelling methods. Unlike indwelling methods, which need experienced and trained

professionals to insert needle sensors beneath human skin, surface EMG (sEMG) methods use patch-like sensors directly placed on human skin. To avoid ethical issues, our experiment was carried out using the sEMG method. Common sEMG signal strength can range from μVs to a few mVs with most of the energy located between 10 and 450 Hz (De Luca, Adam, Wotiz, Gilmore, & Nawab, 2006).

Due to the non-stationary frequency characteristics of EMG signals as reported in Ismail and Asfour (1998), Lau and Wcng (1995) and Rafiee et al. (2009), several time-frequency representation techniques have been studied in the present thesis. Rectification based on signal processing technique features such as advantages, disadvantages and ease of implementation has resulted in the implementation of continuous wavelet transform (CWT). CWT, in which time-frequency (TF) is analysed rather than short-time Fourier transform (STFT), is adopted along with wavelets to realise the measured EMG signals.

Chapter 2: Literature Review

2.1 Neuromuscular systems and Electromyography signals

Electromyography (EMG) signals are electrical signals produced by motor units' activation. These non-stationary signals are normally a function of time and analyzed in terms of their amplitude, frequency and phase. In addition, EMG signals measurement techniques are classified into two types: surface and intramuscular (indwelling). A comparison of the two techniques is shown in Table 1 (AD Instruments, 2010; Stokes, Henry, & Single, 2003; Goreczny, 1995).

Table 1: Comparison of surface and indwelling EMG

	Surface	Indwelling
Electrode type and position	Flat disk: Placed over selected muscle skin.	Needle, fine wire: inserted into selected muscle.
Pick-up zone	Large.	Smaller than surface.
Cross-talk	Significant.	Not significant.
Muscles type	Superficial muscles.	Profound muscles.
usage	Reprehensive of muscle activities.	More selective: good for motor unit studies.

In addition, the cross talk and pick-up zone are positively correlated. This means that the cross-talk is significant if the area of the pick-up zone is large, and vice versa.

The neuromuscular system is complex. An EMG signal is a result of motor unit activation. A Motor unit is α-motor neuron connected to muscle fibers through axon, as shown in figure 1. A single muscle can consist of several hundreds of motor units (De Luca 2008; Hof 1984). Smaller motor units contain smaller motor neurons, fewer fibers and a lower activation threshold; on the other hand, larger motor units have bigger motor neurons, more fibers and a higher activation threshold.

Based on speed, strength and the period of contraction, the motor fibers are classified into: slow twitch and fast twitch. Fast twitch fibers contract quickly and give strength, unlike slow twitch fibers which contract slowly but are used for long time contractions. Moreover, slow twitch fibers have a lower activation threshold than fast twitch fibers. The motor unit contains either slow twitch or fast twitch fibers. However, the entire muscle is a combination of fast and slow motor units (De Luca, 2008; De Luca 2008; Nurco, Conklin, & Shapiro, 2009; Enoka & Stuart, 1984; Seiler, n.d.; Top end sports N.D; Hof 1984).

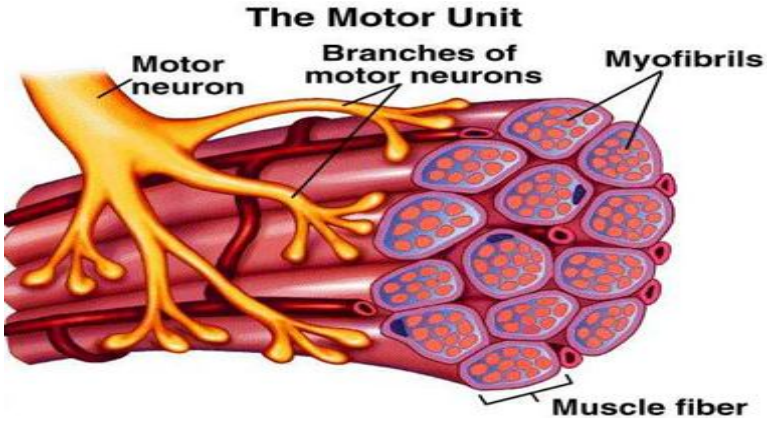

Figure 1: Motor Units configuration (Toxin, 2009)

The motor unit activates and fires an electrochemical impulse when the potential action exceeds the threshold. When the motor unit is activated, an electrochemical impulse is fired,

which is then transmitted from the motor neuron to the fiber, causing the fiber to contract. The transmission mechanism is conducted chemically (De Luca, 2008; De Luca, 2008; Nurco, et al., 2009; Enoka & Staurt, 1984).

2.1.1 The mechanism of motor units' recruitment

The recruitment of motor units is performed based on the size principle and load type (Enoka &Stuart, 1984; Backus et al., 2010; Seiler, n.d.; Hof, 1984). For example, when picking-up something like a pin, a small number of motor units are recruited, but a higher number of motors units are recruited for picking up a heavy table. Furthermore, motor units of a single muscle differ in size, as illustrated in figure 2. Smaller motor units have a lower threshold and they are recruited first. As the load increases, larger motor units are recruited and stronger contraction processes occur.

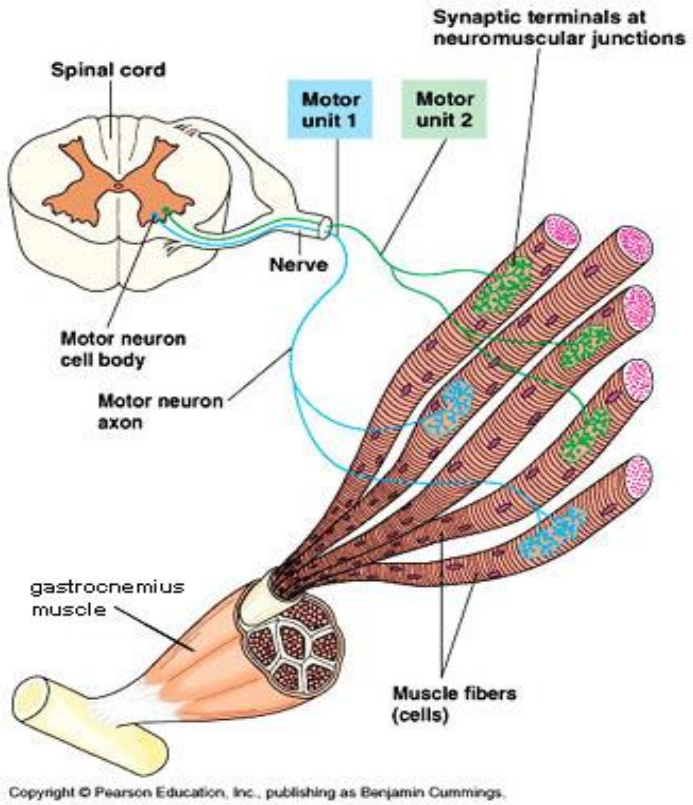

Figure 2: Configuration of neuromuscular system (Toxin, 2009)

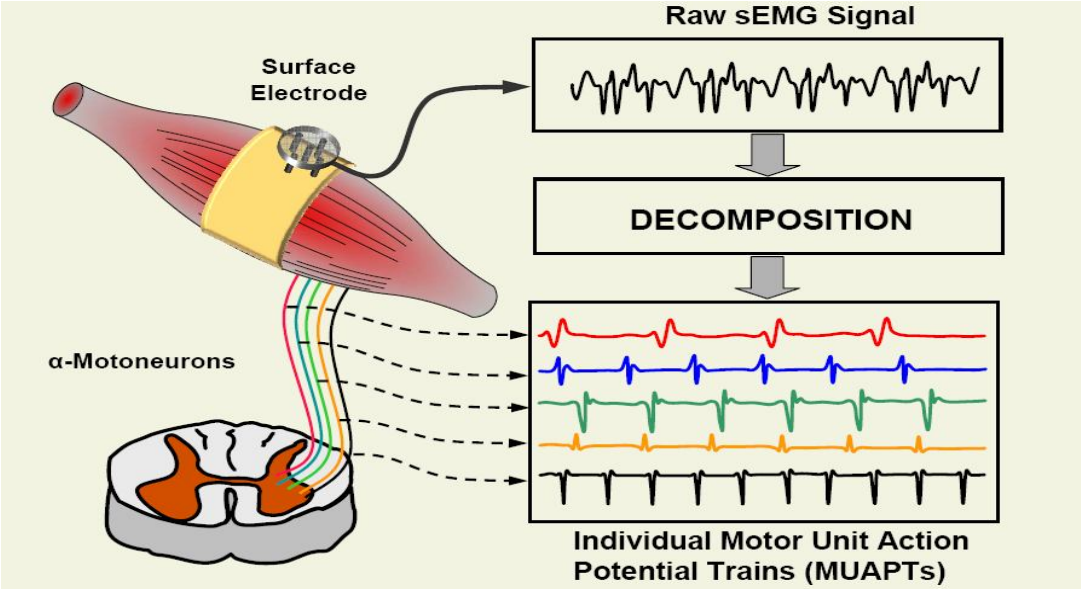

Figure 3: Raw sEMG signal is a sum of multiple Motor units' action potential trains

Raw EMG, detected by surface electrodes, is a sum of fiber signals within the pick-up zone, as shown in figure 3 (De Luca, 2008; De Luca, et al., 2006). Therefore, the feature extraction of sEMG signals is utilized to control the movement of prosthesis. The extraction techniques include statistics (e.g. RMS) of amplitude and frequency coefficients. However, the non-stationary frequency feature of sEMG requires more robust techniques to analyse the signal such as time-frequency analysis.

2.2 Signal Processing Techniques and Feature Extraction Method

Biosignals acquired from human beings are complex and non-stationary. As explained in figure 4, the feature extraction of signals could be performed in the time domain, frequency domain or both time-frequency domains. Several techniques, such as the Hilbert Huang transform and continuous wavelet transform have been developed to deal with non-stationary

and complex signals. This sub-chapter explains three studied time-frequency signal techniques; the Hilbert Huang transform, continuous wavelet transform and short time Fourier transform.

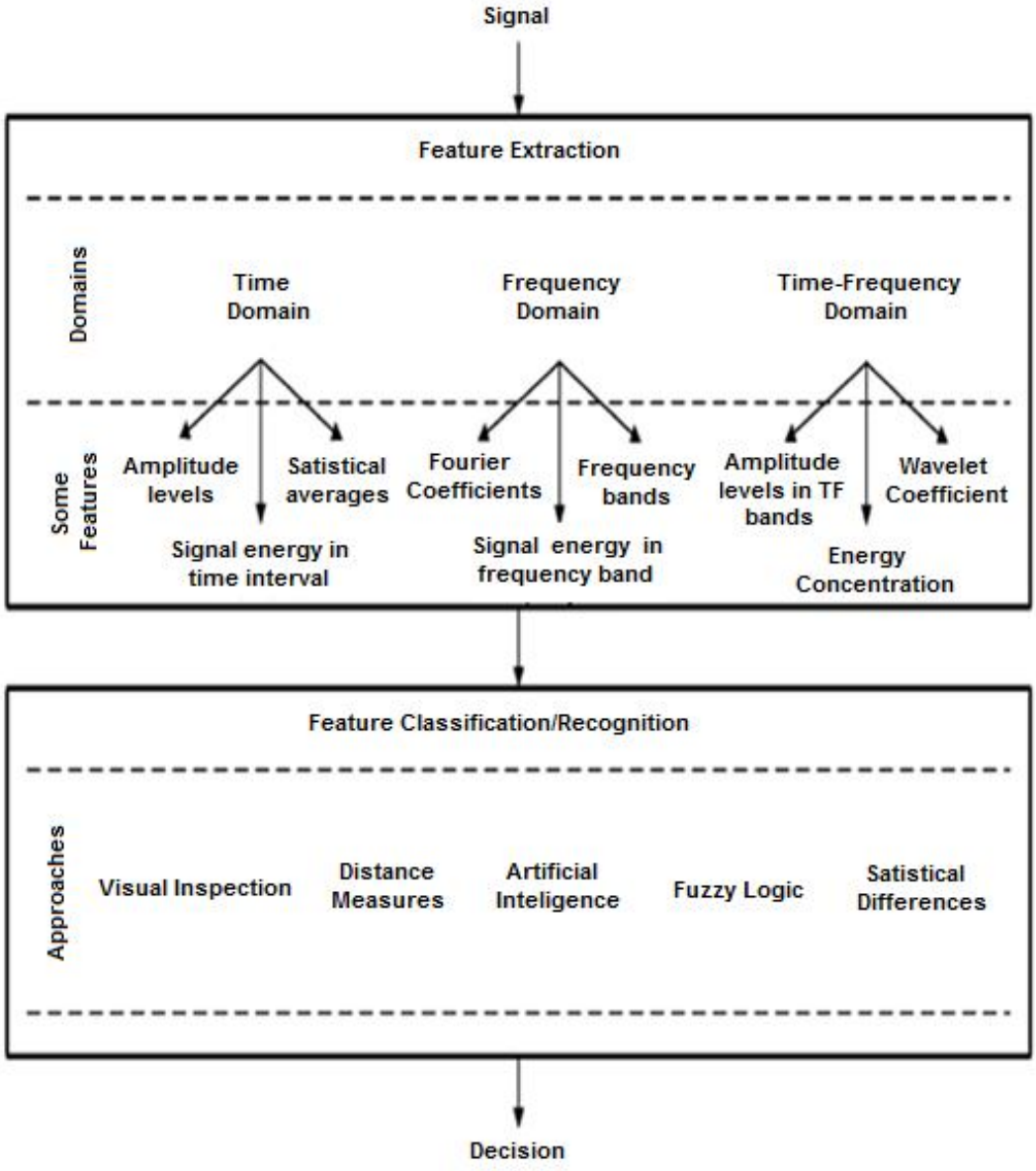

Figure 4: Signal processing for pattern classification in a typical application (Sejdic, Djurovic & Jiang, 2009)

2.2.1 Hilbert Huang Transforms (HHT)

HHT is an integration method of the Empirical Mode Decomposition (EMD) technique and Hilbert Transform (Peng, Tse, & Chu, 2005; Yan & Gao, 2006). Figure 5 explains the methodology of the Hilbert Huang transform (Han, Sun, Wu, & He, 2009).

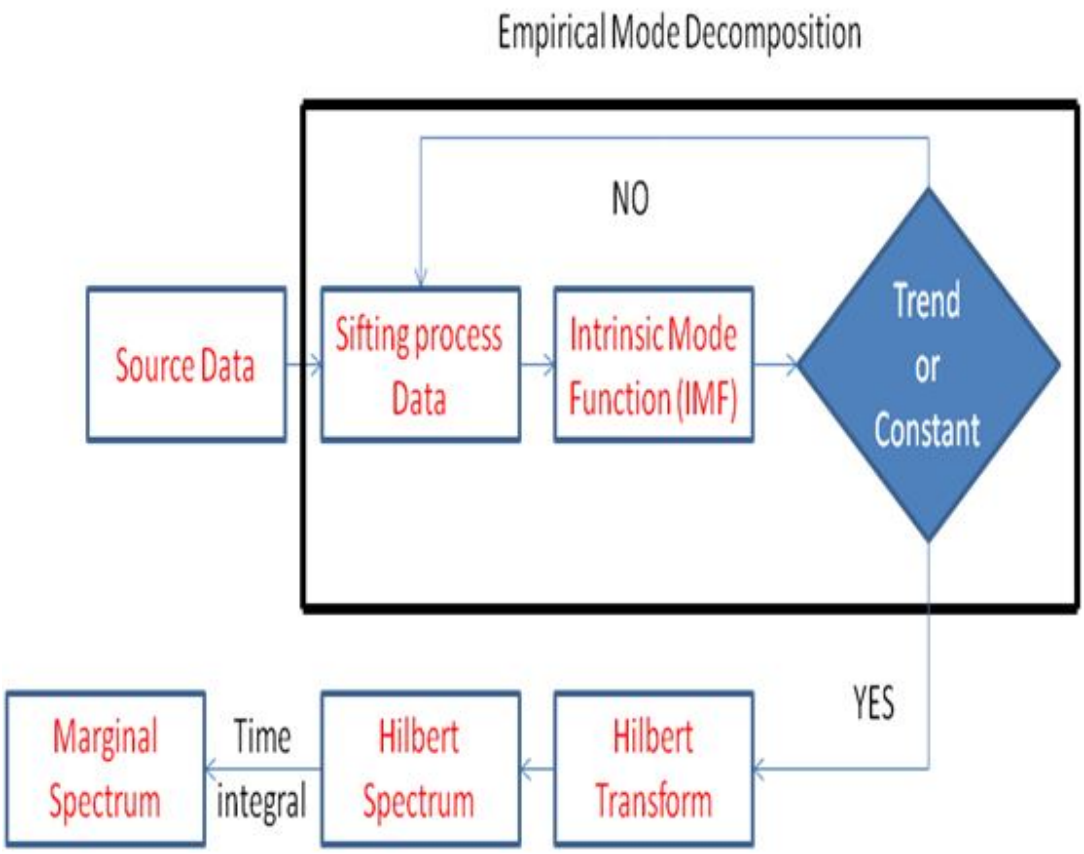

Figure 5: Hilbert Huang Transform flowchart

2.2.1.1 Empirical Mode Decomposition (EMD)

The EMD algorithm decomposes raw signals into the intrinsic mode function (IMF), as explained in figure 6. IMF is, as reported in Yang and Tang (2008), defined as the following:

1- The number of extreme points and zero crossing points must equal or differ by one.
2- The mean value of upper and lower envelop is zero.

2.2.1.2 The EMD algorithm

As reported in Peng, et al. (2005), Huang and Shen (2005), and Agarwal and Tsoukalas (2007), the steps of EMG algorithm are as follows:

1- Identification of local maxima points and minimum points.
2- Connection of all local maxima points by cubic spline line as upper envelop.
3- Connections of all local minima points by cubic spline line as lower envelop.
4- Mean of upper and lower envelop is obtained$\mathrm{m_{nk}}$.
5- The signal is broken down until zero mean is achieved. This is achieved when the stopping criteria SD is < 0.3. (Sometimes <0.2 or 0.1).
6- Once zero mean achieved, IMF ($\mathrm{C_n}$) is assigned to residue ($\mathrm{h_{nk}}$).

Where, K: number of iterations, n: IMF number.

Table 2:Empirical mode Decomposition

	IMF1	**IMF2**	**IMF3**	**…**	**IMF n**
	$X(t)$	$X(t) - C_1 = r_1$	$r_1 - C_2 = r_2$	…	$r_{n-2} - C_{n-1} = r_{n-1}$
0	$X(t) - m_1 = h_1$	$r_1 - m_2 = h_2$	$r_2 - m_3 = h_3$	…	$r_2 - m_n = h_n$
1	$h_1 - m_{11} = h_{11}$	$h_2 - m_{21} = h_{21}$	$h_3 - m_{31} = h_{31}$	…	$h_n - m_{n1} = h_{n1}$
2	$h_{11} - m_{12} = h_{12}$	$h_{21} - m_{22} = h_{22}$	$h_{31} - m_{32} = h_{32}$	…	$h_{n1} - m_{n2} = h_{n2}$
3	$h_{12} - m_{13} = h_{13}$	$h_{22} - m_{23} = h_{23}$	$h_{32} - m_{33} = h_{33}$	…	$h_{n2} - m_{n3} = h_{n3}$
…	….	….	….	…	….
k	$h_{1(k-1)} - m_{1k} = h_{1k}$	$h_{2(k-1)} - m_{2k} = h_{2k}$	$h_{3(k-1)} - m_{3k} = h_{3k}$	…	$h_{n(k-1)} - m_{nk} = h_{nk}$
IMF	$h_{1k} = C_1$	$h_{2k} = C_2$	$h_{3k} = C_3$	…	$h_{nk} = C_n$

Sifting Process

The Mathematical description shown in the steps above are explained in EMD algorithm equations in table 2.

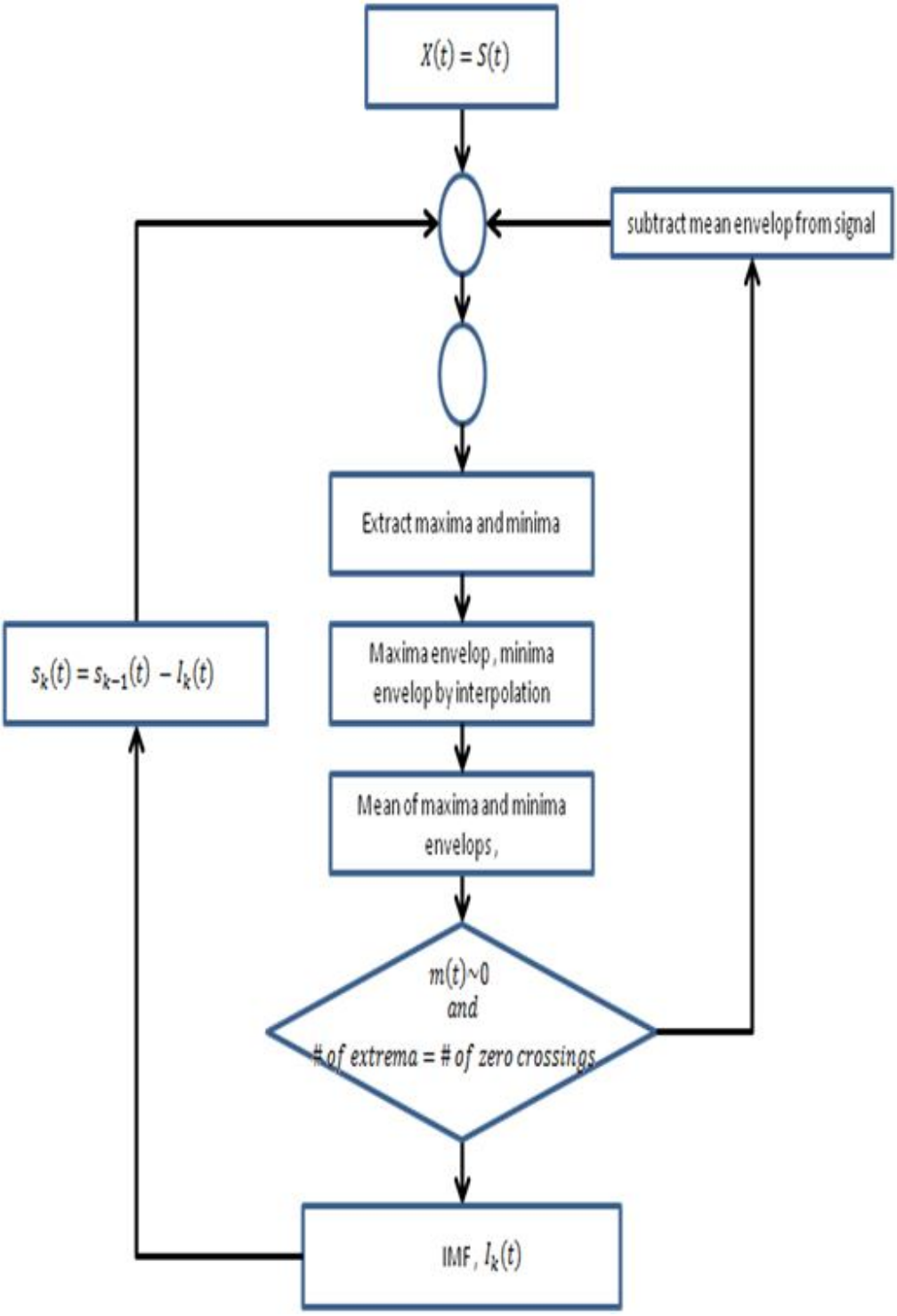

Figure 6: Empirical Mode Decomposition flowchart (Feng, Ding, & Jiang, 2010; Yu, Cheng, & Yang, 2005; Yan & Gao, 2006)

As reported in Han et al. (2009) and Agarwal and Tsoukalas (2007), the stopping criteria equation is given by:

$$SD \geq \sum_{t=0}^{T} \frac{|h_{1(K-1)}(t) - h_{1k}(t)|^2}{h_{1(k-1)}^2(t)} \quad \textbf{(1)}$$

They also report that the original signal is a sum of IMFs and last residue, given by:

$$X(t) = \sum_{i=1}^{n} C_i + r_n \quad \textbf{(2)}$$

2.2.1.3 Hilbert Transform

Hilbert transform is a linear operator which transforms a particular function into another function within the same domain. The function, as reported in Peng et al. (2005), is given by:

$$\mathrm{y(t)} = \frac{\mathrm{P}}{\pi}\int_{-\infty}^{\infty} \frac{\mathrm{x(\tau)}}{\mathrm{t-\tau}}\,\mathrm{d\tau} \quad , \qquad \mathrm{P: Cauchy\ principal\ value} \quad \textbf{(3)}$$

$$z(t) = x(t) + iy(t) = a(t)e^{i\theta(t)} \quad \textbf{(4)}$$

Where, $\mathrm{a(t)}$ is the instantaneous amplitude function, and $\Theta\mathrm{(t)}$ is the phase function.

The instantaneous amplitude function and the phase functions are described by:

$$a(t) = \sqrt{x(t)^2 + y(t)^2} \quad \textbf{(5)}$$

$$\Theta(t) = tan^{-1}(\frac{y}{x}) \quad \textbf{(6)}$$

The instantaneous frequency function is a time derivative of the phase function, and it is given by:

$$\omega(t) = \frac{d\Theta(t)}{dt} \quad \textbf{(7)}$$

2.2.2 Continuous Wavelet Transform (CWT)

2.2.2.1 Introduction to CWT

This applies convolution techniques to divide a continuous time function into a time-frequency domain (Alsberg, Kell, & Woodward, 1997; Torrence and Compo, 1998; Rafiee et al., 2009; Addison, 2002; Mallat, 1998). The function is given by:

$$X_w(a,b) = \frac{1}{\sqrt{a}}\int_{-\infty}^{\infty} x(t)\,\psi^*\left(\frac{t-b}{a}\right)dt \quad a,b \in \mathcal{R}, a > 0 \quad \textbf{(8)}$$

Where, $\boldsymbol{a}$ is a scale parameter, $\boldsymbol{b}$ is a translation parameter, and $\boldsymbol{\psi}^*$ is the conjugate of $\boldsymbol{\psi}$. The scale is inversely proportional to frequency; a large scale value gives a small frequency and vice versa. The relationship and pseudo frequency equation is given by Rajagopalan and Ray (2006):

$$f = \frac{f_c\, f_s}{a} \quad \textbf{(9)}$$

Where, $\boldsymbol{f_c}$ is a wavelet central frequency, and $\boldsymbol{f_s}$ is the sampling frequency. The pass band centre of energy spectrum($\boldsymbol{f_c}$) is derived from the second moment of the energy spectrum area. The equation, as reported in Addison (2002), is given as follows:

$$f_c = \sqrt{\frac{\int_0^\infty f^2 |\psi(f)|^2}{\int_0^\infty |\psi(f)|^2}} \quad \textbf{(10)}$$

2.2.2.2 Mother wavelet requirement

As described in Alsberg et al. (1997), Torrence and Compo (1998), Rafiee et al. (2009), Addison (2002), Grigoryan (2005) and Mallat (1998), the mother wavelet of $\boldsymbol{\psi(t)}$ must satisfy the following requirements:

1- Finite energy ($\boldsymbol{L^2\ hilbert\ Space}$)

$$E = \int_{-\infty}^{\infty} |\psi(t)|^2 \ dt < \infty \quad \textbf{(11)}$$

$$E = \int_{-\infty}^{\infty} |\psi(t)|^2 \ dt = \int_{-\infty}^{\infty} |\psi(f)|^2 \ df \quad \textbf{(12)}$$

$$Normalized\ Wavlet = \frac{1}{\sqrt{E}}\psi(t)$$

If ψ(t) is a complex function, the magnitude must be calculated using both its real and complex parts. Moreover, the Fourier transform of a complex wavelet must be both real and vanish for negative frequencies.

2- Admissibility constant

$$C_g = \int_0^\infty \frac{|\psi(f)|^2}{f} \ df < \infty \quad \textbf{(13)}$$

The value of C_g depends on the chosen wavelet. The corresponding Fourier transform of a wavelet is therefore:

$$\tilde{\psi}(f) = \int_{-\infty}^{\infty} \psi(t)\ e^{-i2\pi ft}\ dt\ \ , \tilde{\psi}(0) = 0 \quad \textbf{(14)}$$

When $\tilde{\boldsymbol{\psi}}(\boldsymbol{f})$ has a zero frequency component, this implies a zero mean in the time domain, given by the function:

$$\int_{-\infty}^{\infty} \psi(t)\ dt = 0 \quad \textbf{(15)}$$

2.2.2.3 Uncertainty (time resolution and frequency resolution)

The Heisenberg Uncertainty Principle, figure 7, defines the lower limit of time-frequency window resolution. The function, as reported in Mallat (1998), Norman and Lai (2007), Wei and Pei-Wen (2009), and Kiymik, Güler, Dizibüyük, and Akin (2004), is given by:

$$\Delta f_w\, \Delta t_w \geq\ constant \quad \textbf{(16)}$$

$$constant\ (f) = \frac{1}{4\pi}\ \ or\ \ \ constant(\omega) = \frac{1}{2}$$

U.S

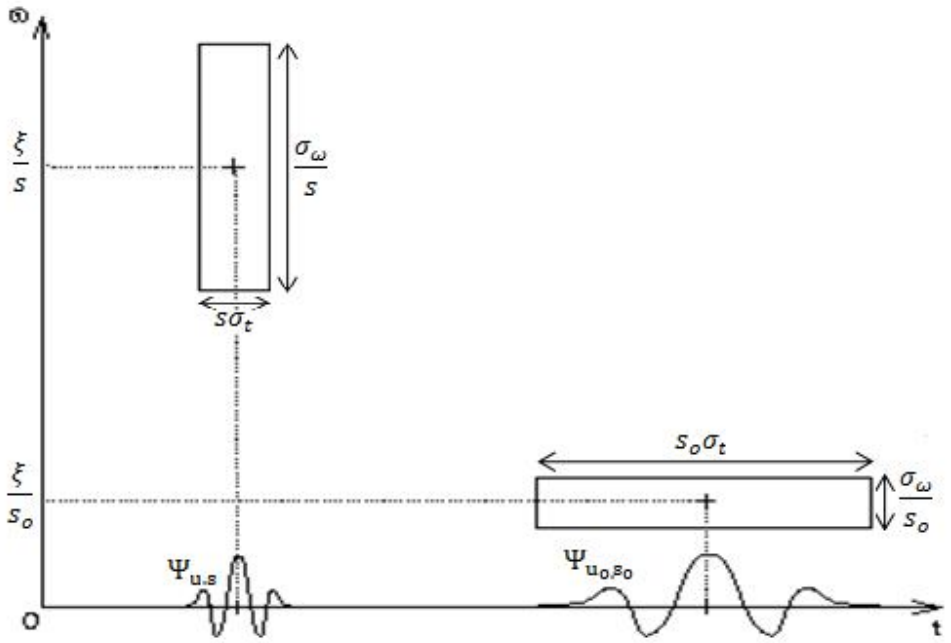

Figure 7: Heisenberg Box of different time-frequency resolutions of a wavelet

Where, Δf_w is a frequency window width parameter, and Δt_w a time window width parameter. Their functions are given by:

$$\Delta f_w = \sqrt{\frac{1}{E}\int_{-\infty}^{\infty}(f - f_0)^2 . |\psi(f)|^2 df} \quad \textbf{(17)}$$

$$\Delta t_w = \sqrt{\frac{1}{E}\int_{-\infty}^{\infty}(t - t_0)^2 . |\psi(t)|^2 dt} \quad \textbf{(18)}$$

Where, f_0 and t_0 are windows centres in the frequency and time domains, respectively. Their functions are defined by:

$$f_0 = \frac{1}{E}\int_{-\infty}^{\infty} f.|\psi(f)|^2 \ df \quad \textbf{(19)}$$

$$t_0 = \frac{1}{E}\int_{-\infty}^{\infty} t.|\psi(t)|^2 \ dt \quad \textbf{(20)}$$

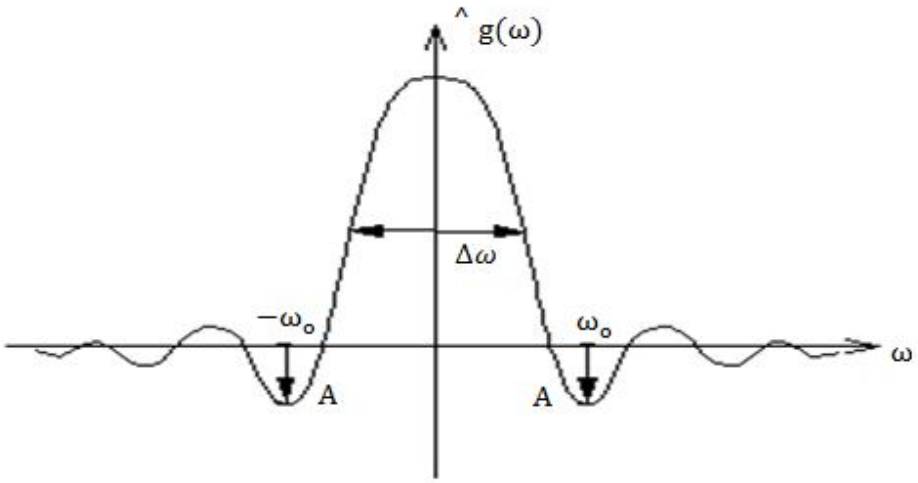

Figure 8: Bandwidth and central frequency

Short Fourier transform has constant bandwidth and time resolution (figure 9), unlike wavelet transform which has variable time and frequency resolution (figure 10). However, another dimension which is used in wavelet transform is called **Quality Factor**. It determines whether the mother wavelet is linearly or nonlinearly scaled (Chen & Zhang, 2005; Von Tscharner, 2000; Yao and Zhang, 2001; Kiymik et al., 2004). The function is described by:

$$Q = \frac{f}{B} \quad \textbf{(21)}$$

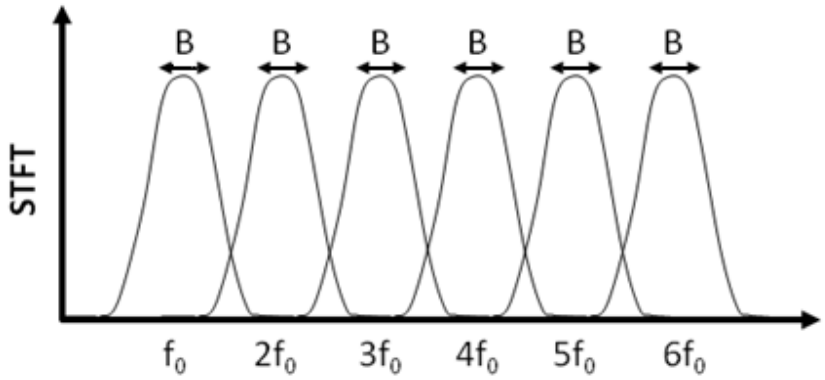

Figure 9: Bandwidth vs. Central frequency of STFT

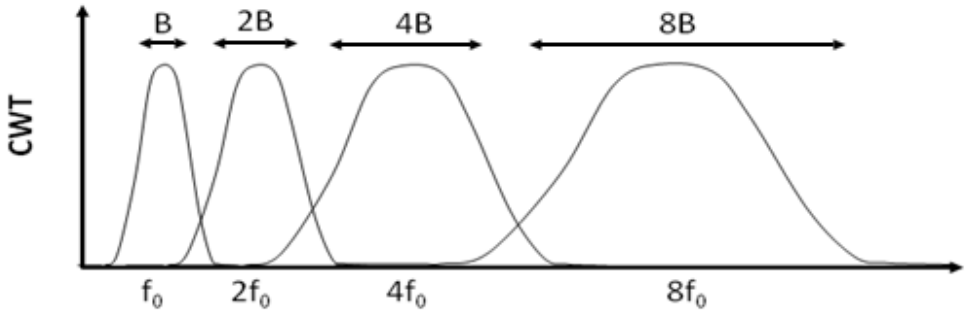

Figure 10: Bandwidth vs. Central frequency of CWT (Lee, Lee, Kim, Min & Hong, 1999)

Von Tscharner (2000) introduced a novel method by developing nonlinear scaling wavelet (based on Cauchy wavelet), as shown in figure 11. This means that the Q value is a variable. The wavelets were developed in the frequency domain, and the wavelets in the time domain were derived by applying the inverse Fourier transform (Von Tscharner, 2000). As well as Tscharner's wavelet, complex Morlet wavelet and complex Shannon wavelet could be considered as nonlinear scaled wavelets.

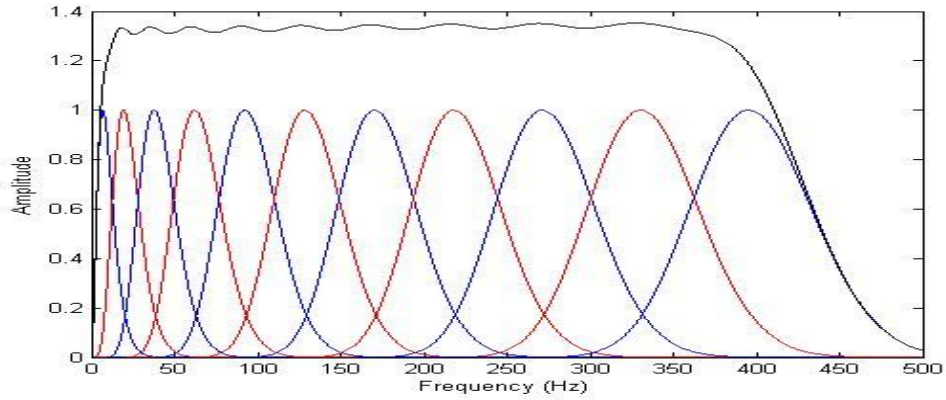

Figure 11: Nonlinear scaling wavelet

2.2.2.4 Mother Wavelet vs. Father Wavelet (scaling wavelet)

The main difference between a mother wavelet and a scaling function is that a mother wavelet behaves as a band pass filter while a scaling function acts as a low pass filter.

2.2.2.5 Mother Wavelet Types

There are different types of mother wavelets (Addison, 2002; Torrence and Compo, 1998; Daubechies 1991; Scheper & Teolis, 2003; Teolis, 1998; Mallat, 1998). The following wavelets are the ones this research will focus on (refer to section two of appendices for all mathematical derivation of equations and constants in this section).

2.2.2.5.1 Mexican hat wavelet

This is one of the most known wavelets. It is the negative normalized second derivative of a Gaussian function with an admissibility constant value of $\boldsymbol{\pi}$, and symmetric with effective support between 5 and -5 (Addison, 2002; Kiymik et al., 2004). It is only used in continuous transform (Figure 12). The equation is given by:

$$\psi(t) = (1 - t^2)e^{\frac{-t^2}{2}} \quad \textbf{(22)}$$

The corresponding Fourier transform is given by equation (23). Figure 13 shows the energy spectrum of the frequency domain equation of the Mexican hat wavelet.

$$\hat{\psi}(\omega) = \sqrt{2\pi}\omega^2 e^{\frac{-\omega^2}{2}} \quad \textbf{(23)}$$

The normalization factor is derived based on $2^{\text{nd}} - \text{norm}$ in Hilbert space L^2. Therefore:

$$E = \int_{-\infty}^{\infty} \psi(t)^2\, dt = \int_{-\infty}^{\infty} \left[(1-t^2)e^{\frac{-t^2}{2}}\right]^2 dt = \frac{3}{4}\sqrt{\pi} \quad \textbf{(24)}$$

$$E = \int_{-\infty}^{\infty} \left|\hat{\psi}(f)\right|^2 df = \int_{-\infty}^{\infty} 32\pi^5 f^4 e^{-4\pi^2 f^2}\, df = \frac{3}{4}\sqrt{\pi} \quad \textbf{(25)}$$

The Normalized-energy Mexican hat equation is given by:

$$\psi(t) = \frac{1}{\sqrt{E}}(1-t^2)e^{\frac{-t^2}{2}} = \frac{2}{\sqrt{3}\sqrt[4]{\pi}}(1-t^2)e^{\frac{-t^2}{2}} \quad \textbf{(26)}$$

The CWT of Mexican hat is given by:

$$\psi\left(\frac{t-b}{a}\right) = \left[1-\left(\frac{t-b}{a}\right)^2\right] e^{\frac{-\left(\frac{t-b}{a}\right)^2}{2}} \quad \textbf{(27)}$$

$$T(a,b) = \frac{1}{\sqrt{a}}\int_{-\infty}^{\infty} x(t)\, \psi^*\left(\frac{t-b}{a}\right) dt \quad \textbf{(28)}$$

$T(a,b) = CWT\ coeffecient\ ,\quad x(t)\text{: }source\ signal$

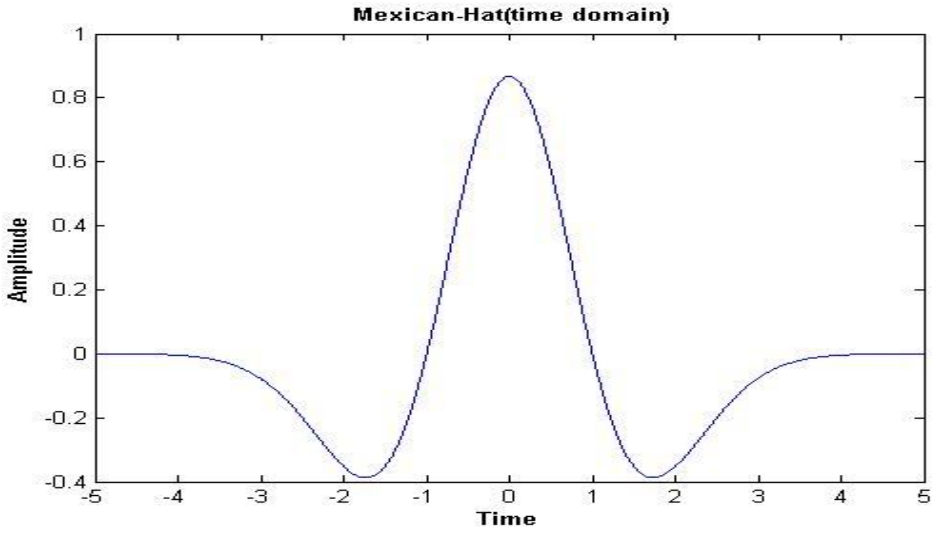

Figure 12: Mexican hat (time domain)

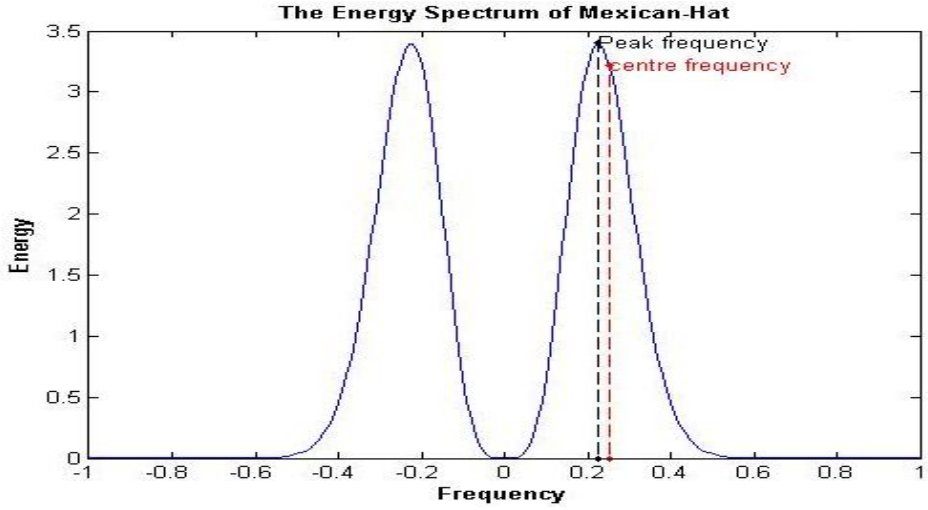

Figure 13: Energy spectrum of Mexican hat (frequency domain), central frequency is 0.251 Hz (see section two of appendices)

2.2.2.5.2 Derivative of Gaussian (DOG) wavelets

The DOG wavelet is symmetric and used in continuous transform. DOG equation, in the time domain, is given by Torrence and Compo (1998):

$$\psi(t) = \frac{(-1)^{m+1}}{\sqrt{\Gamma\left(m+\frac{1}{2}\right)}} \frac{d^m}{dt^m}\left(e^{-\frac{t^2}{2}}\right), \quad m = derivaitve \tag{29}$$

The corresponding Fourier transform of DOG is therefore:

$$\hat{\psi}(s\omega) = \frac{(i)^m}{\sqrt{\Gamma\left(m+\frac{1}{2}\right)}} (s\omega)^m e^{\frac{-(s\omega)^2}{2}} \tag{30}$$

Figure 14 shows the plot of the 5th derivative of Gaussian wavelet in the time domain.

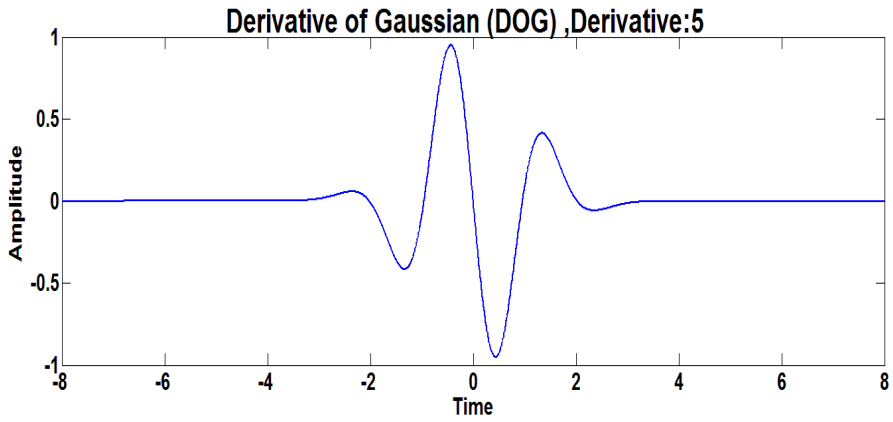

Figure 14: 5th -DOG (time domain)

2.2.2.5.3 Derivative of Complex Gaussian (DOCG) wavelets

The DOCG wavelet is symmetric and used in complex continuous transform. The time domain equation of DOCG wavelet is given by Teolis (1998):

$$\psi(t) = C_m \frac{d^m}{dt^m}\left(e^{-it}e^{-t^2}\right), \quad m = derivaitve \tag{31}$$

C_m: $normalisation\ factor\ \ such\ that\ ||\psi(t)||^2\ equal\ 1$

Figure 15 shows the plot of the 8th derivative of complex Gaussian wavelet in the time domain.

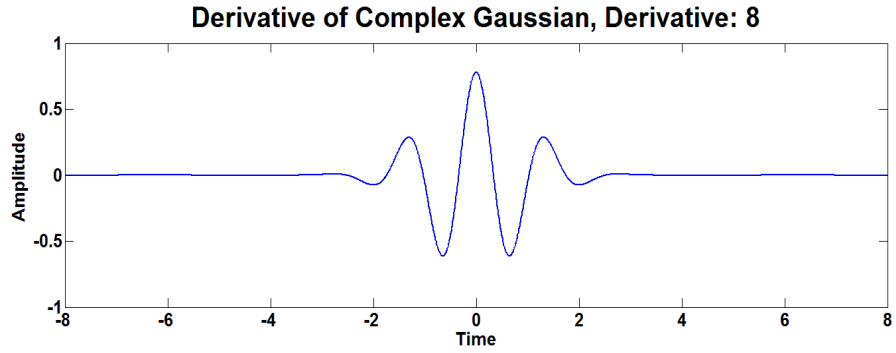

Figure 15: 8th -DOCG (time domain)

DOG and DOCG wavelets vary in central frequencies along with the derivative order (see section four of appendices). Therefore, they have different scales for a particular frequency.

2.2.2.5.4 Complex Morlet wavelet

The complex Morlet wavelet is a product of the complex sinusoidal function and the Gaussian function. The complex Morlet wavelet is symmetric and used in complex continuous transform,

as the example given in figure 16 portrays. The equation is given by Teolis (1998) and Norman and Lai (2007):

$$\psi(t) = \frac{1}{\sqrt{\pi f_b}} e^{2\pi i f_c t} e^{\frac{-t^2}{f_b}} \quad \textbf{(32)}$$

Where, f_c is the central frequency and f_b is the frequency bandwidth. The normalization factor is derived based on the first-dimension, L, of Hilbert space.

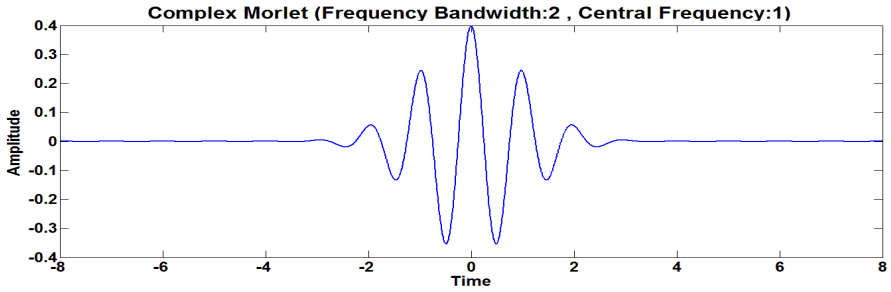

Figure 16: Complex Morlet (time domain)

The corresponding Fourier transform without the normalization factor is given by:

$$g(f) = \sqrt{\pi f_b} e^{\frac{-f_b}{4}(2\pi f - 2\pi f_c)^2} \quad \textbf{(33)}$$

2.2.2.5.5 Meyer wavelet

The Meyer wavelet is symmetric within an effective support [8,-8]. The wavelet function is defined in the frequency domain, and it is given by:

$$\hat{\psi}(\omega) = (2\pi)^{-1/2} e^{i\omega/2} sin\left(\frac{\pi}{2} v\left(\frac{3}{2\pi}|\omega| - 1\right)\right) \quad if \quad \frac{2\pi}{3} \leq |\omega| \leq \frac{4\pi}{3}$$

$$\hat{\psi}(\omega) = (2\pi)^{-1/2} e^{i\omega/2} cos\left(\frac{\pi}{2} v\left(\frac{3}{4\pi}|\omega| - 1\right)\right) \quad if \quad \frac{4\pi}{3} \leq |\omega| \leq \frac{8\pi}{3}$$

Where, $v(a) = a^4(35 - 84a + 70a^2 - 20a^3)$ $\quad a \in [0,1]$ **(34)**

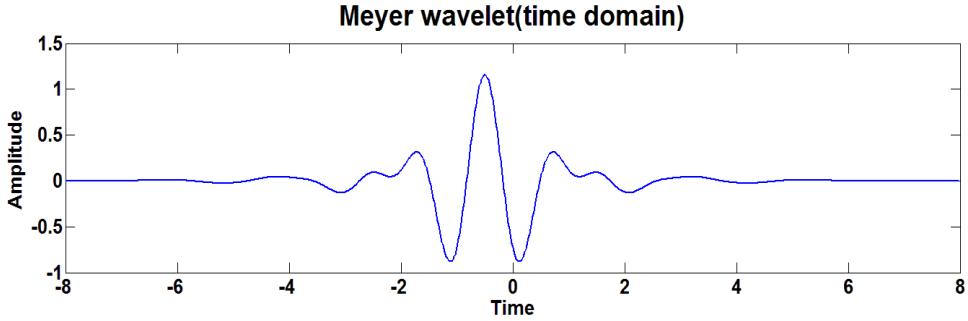

Figure 17: Meyer wavelet (time domain)

2.2.2.5.6 Complex Shannon wavelet

The complex Shannon wavelet is a product of complex sinusoidal functions and sinc functions. The complex Shannon wavelet is symmetric and used in complex continuous transform, as the example given in figures 19 and 20 shows the equation is given by Teolis (1998):

$$\psi(t) = \sqrt{f_b} sinc(f_b t) e^{2\pi i f_c t} \quad \textbf{(35)}$$

Where, f_c is the central frequency and f_b is the frequency bandwidth. In the frequency domain, the complex Shannon wavelet is a rectangular pulse centered in $f_c$and with a width proportional to the parameter f_b, as illustrated in figure 18.

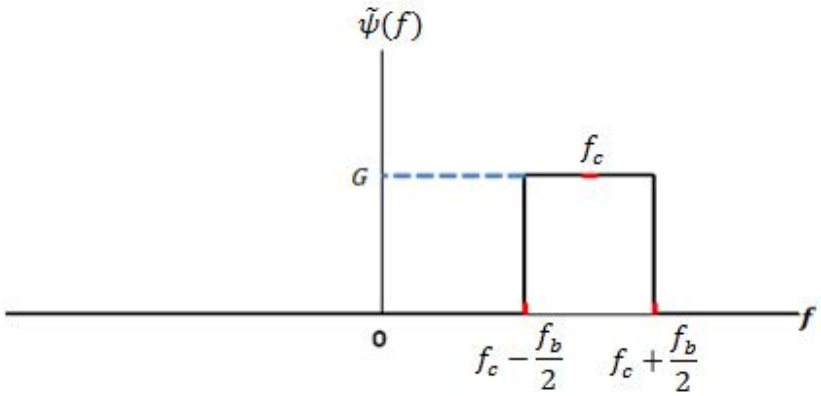

Figure 18: Complex Shannon wavelet (frequency domain)

The frequency domain equation (Costa & de Matos, 2008) is defined as:

$$\tilde{\psi}(f) = \begin{Bmatrix} G, \text{if } f_c - \frac{f_b}{2} \leq f \leq f_c + \frac{f_b}{2} \\ 0\ , \text{otherwise} \end{Bmatrix} \quad \textbf{(36)}$$

Where, G is the gain.

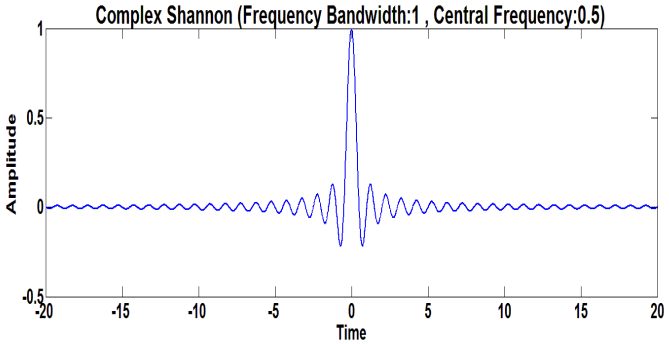

Figure 19: Complex Shannon, low central frequency (time domain)

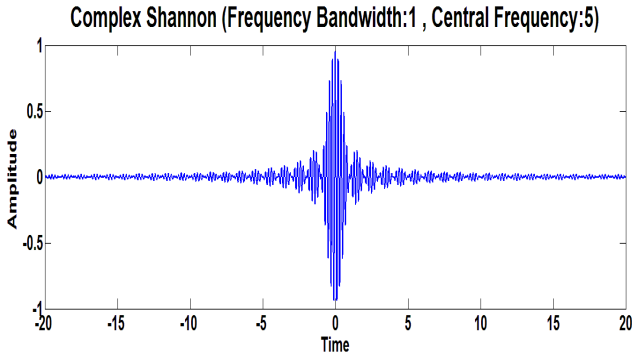

Figure 20: Complex Shannon, high central frequency (time domain)

2.2.2.5.6 Daubechies, Symlets, and Coiflets wavelet family

The Daubechies, Symlets and Coiflets wavelets (Figures 21, 22 and 23) are multi resolution-based wavelets developed mainly by Ingrid Daubechies. However, they could be used in continuous and discrete transform. Unlike Daubechies wavelets which are asymmetric, Symlets and Coiflets are nearly symmetric. They all compactly support orthogonal wavelets (Mallat, 1998; Daubechies, 1991; Kaiser, 1995). Furthermore, although the generating functions of these wavelets are complex, they principally satisfy the following basic properties:

- Zero mean property:

$$\sum_{n=0}^{N-1} h[n] = 0 \quad \textbf{(37)}$$

- Energy normalization property:

$$\sum_{n=0}^{N-1} h[n]^2 = 1 \quad \textbf{(38)}$$

- Wavelet Filter Bank (WFB) orthogonality property:

$$\sum_{n=0}^{N-1} h[n]h[n+2l] = 0 \quad \textbf{(39)}$$

- Fourier Transform:

$$\hat{h}(\omega) = \sum_{n=0}^{N-1} h[n]e^{-in\omega} \quad \textbf{(40)}$$

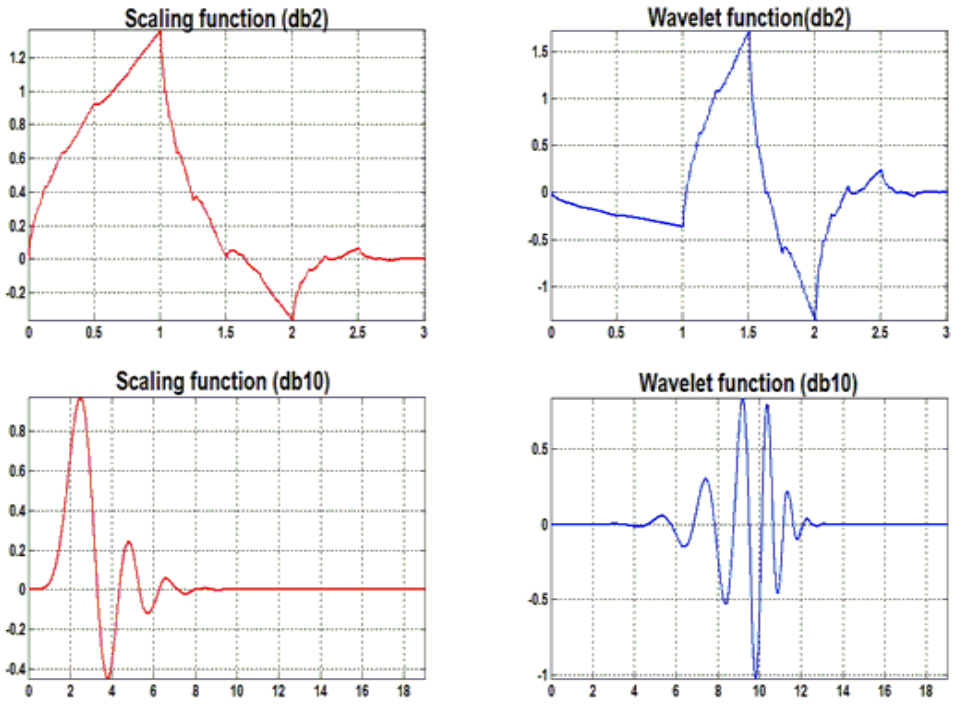

Figure 21: Daubechies family (order 2 and 10)

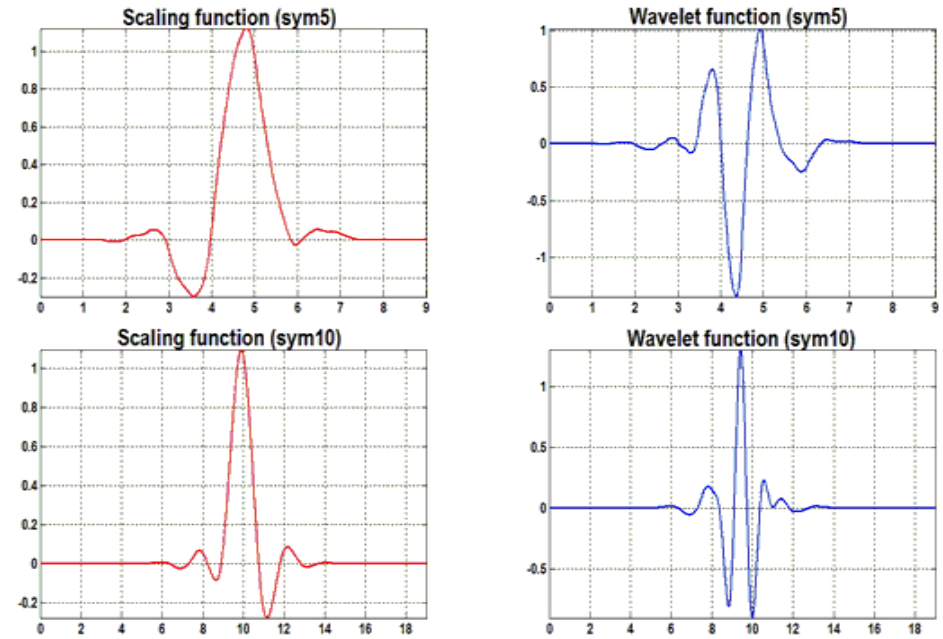

Figure 22: Symlets family (order 2 and 10)

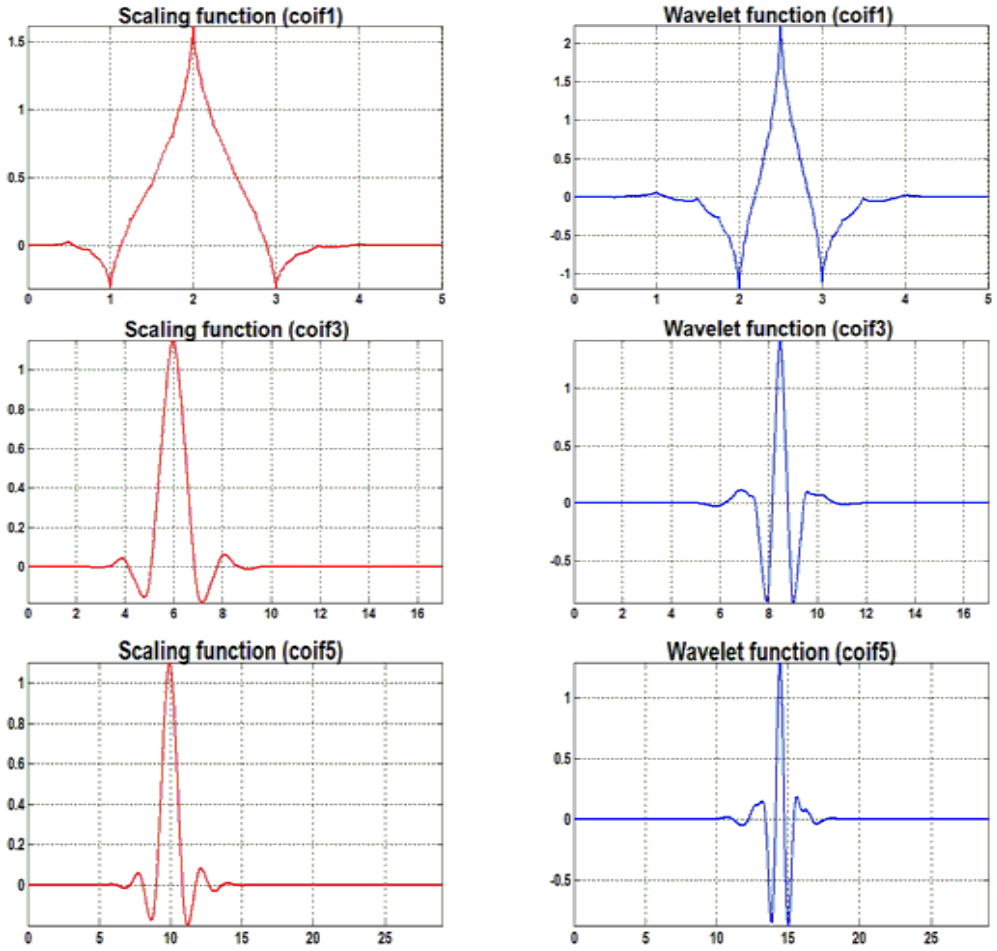

Figure 23: Coiflets family (order 2 and 10)

2.2.3 Short Time Fourier Transform (STFT)

The STFT equation (Addison, 2002; Wen & Qiang, 2009; Lee et.al., 1999; Kiymik et al., 2004) is expressed by:

$$F(f,b) = \int_{-\infty}^{\infty} X(t)h(t-b)\, e^{-i2\pi ft}dt \quad \textbf{(41)}$$

Where, $h(t-b)$a window function and b is a translation parameter.

The types of windows are Hanning, Hamming, cosine, Kaiser, Gaussians, etc. The most common STFT is the Gabor Transform (Addison, 2002). The Gabor Transform (GT), Gaussian windowed STFT, is given by:

$$h(t) = \frac{1}{\sqrt{\sigma}\pi^{\frac{1}{4}}} e^{\frac{-1}{2}(t^2/\sigma^2)} \quad \textbf{(42)}$$

$$h(t-b) = \frac{1}{\sqrt{\sigma}\pi^{\frac{1}{4}}} e^{\frac{-1}{2}((t-b)^2/\sigma^2)} \quad \textbf{(43)}$$

$$G_x(t,f) = \int_{-\infty}^{\infty} X(t) \frac{1}{\sqrt{\sigma}\pi^{\frac{1}{4}}} e^{\frac{-1}{2}((t-b)^2/\sigma^2)}\, e^{-i2\pi ft}dt \quad \textbf{(44)}$$

2.2.4 Comparison of signal processing techniques

Table 3 explains the differences between the short-time Fourier transform (STFT), Wavelet transform (WT) and Hilbert Huang transform (HHT) (Peng, et al., 2005; Huang & Shen, 2005).

Table 3: Comparison between STFT, WT and HHT

	STFT	WT	HHT
Basis	Non-adaptive	Non-adaptive	Adaptive
Frequency	**convolution:** global, uncertainty	**convolution:** regional, uncertainty	**differentiation:** local, certainty
Presentation	energy-time-frequency	energy-time-frequency	energy-time-frequency
Non-linear	No	No	Yes
Non-stationary	Yes (fixed resolution)	Yes (variable resolution)	Yes
Feature Extraction	Discrete: No Continuous: Yes	Discrete: No Continuous: Yes	Yes
Theoretical base	theory complete	theory complete	Empirical

2.2.4.1 Engineering judgment of the best signal processing technique

Due to non-stationary frequency characteristics of EMG signals, the wavelet transform (WT) and Hilbert Huang transform (HHT) have been implemented widely as a time-frequency analysis tool rather than short-time Fourier transform because of their variable time-frequency resolutions as shown in figure 24 and table 3 (Yao & Zhang, 2001). Moreover, HHT is better in dealing with nonlinear signals than WT. However, the iterations of breaking down the signal using EMD take long computation, especially for a signal that has many frequency components such as EMG. Therefore, WT is considered as a TF signal processing tool for EMG, although it does not maintain absolute phase of the signal components. It does not have any impact in the proposed experiment, and scale to frequency conversion is dependent on a mother wavelet (Sejdic et al., 2009).

Due to data redundancy, continuous wavelet transform has the ability over discrete wavelet Transform to distinguish the signal content, (Xie & Ding, 2009; Kiymik et al., 2004).

As well as the above three signal processing, there are many Time-Frequency representations such as the Wigner-Ville Distribution (WVD). However, WVD has a cross term problem; it is basically not an efficient TFA tool for multi-component signals (Liu et al., 2005).

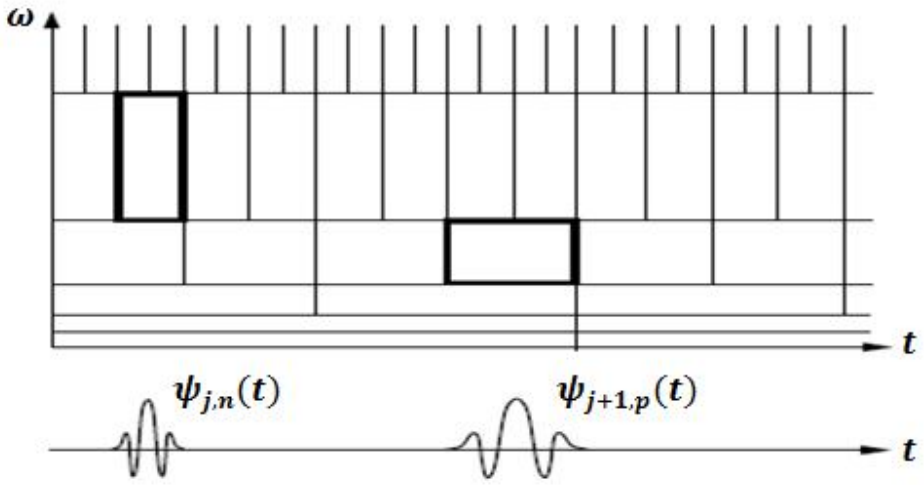

Figure 24: Variable resolution of time and frequency in wavelet transform

2.3 Feature Extraction analysis

2.3.1 Introduction

The larger the entropy value, the more energy distribution and higher uncertainty prediction are observed. Uncertainty, complexity and disorder of energy distribution over the wavelet coefficients are quantified by the "entropy" parameters as:

$S = -\sum_{i=1}^{N} P_i \, log_e \, P_i$, Where P_i is the probability of a given sample. **(45)**

In general, as shown in Mishra, özger, and Singh (2009), Zhengyou and Qingquan (2007), Zheng-You, Xiaoqing, and Guoming (2006), Lee, He, Ilhan, Linscott and Olgin (2005) and Von Tscharner (2000), entropy value is proportional to uncertainty measures with two independent measurements named Wavelet time entropy (WTE) and Wavelet frequency entropy (WFE), where the energy for WFE at each scale *j* is given by:

$$E_j = \sum_{k=1}^{N} |C_k(j)|^2 \quad \textbf{(46)}$$

With a corresponding probability at each scale *j* as:

$$P_j = \frac{|C_k(j)|^2}{E_j} \quad \textbf{(47)}$$

Whereas the energy for WTE at each time sample *k* is written as:

$$E_k = \sum_{j=1}^{J} |C_j(k)|^2 \quad \textbf{(48)}$$

And therefore its probability at the time sample *k* is:

$$P_k = \frac{|C_j(k)|^2}{E_k} \quad \textbf{(49)}$$

The TF representation is configured with the horizontal axis being the sample in time, and the vertical axis spotted as the frequency value. Therefore along with this configuration, WTE and WFE values in this study are both illustrated on the same graph as shown in figure 25. The desired scale range is from 10Hz to 200 Hz.

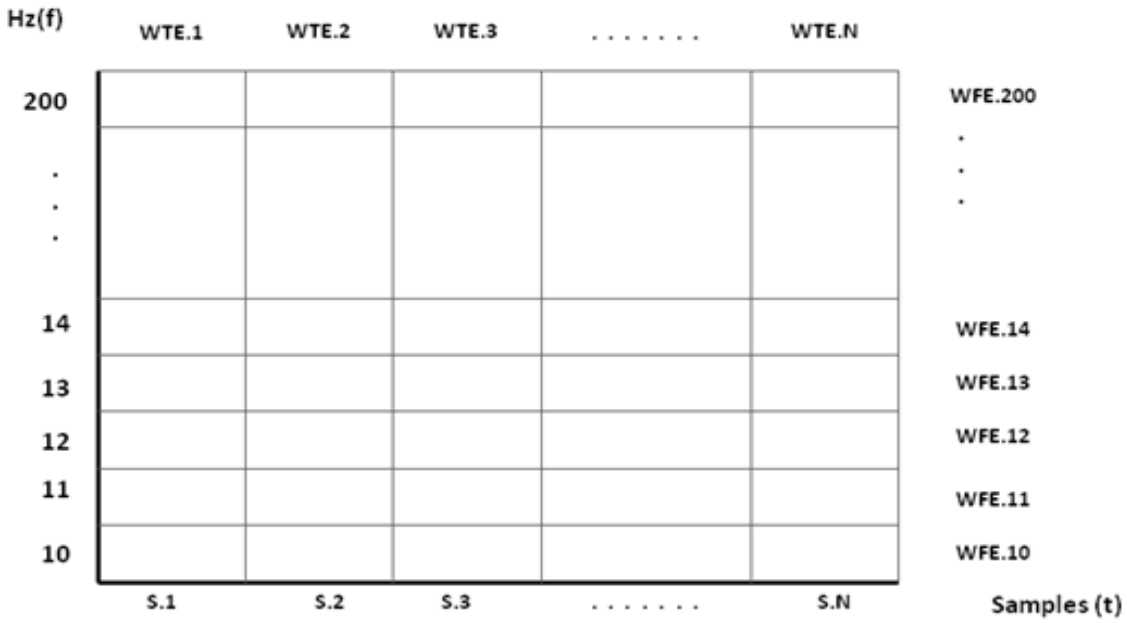

Figure 25: Picture of implementation of WTE and WFE. (WTE.X, X: sample number, WFE.Y: Y: Frequency)

Chapter 3: Experiment Design and Setup

Figure 26 demonstrates the flow visualization of literature review (Experiment Design).

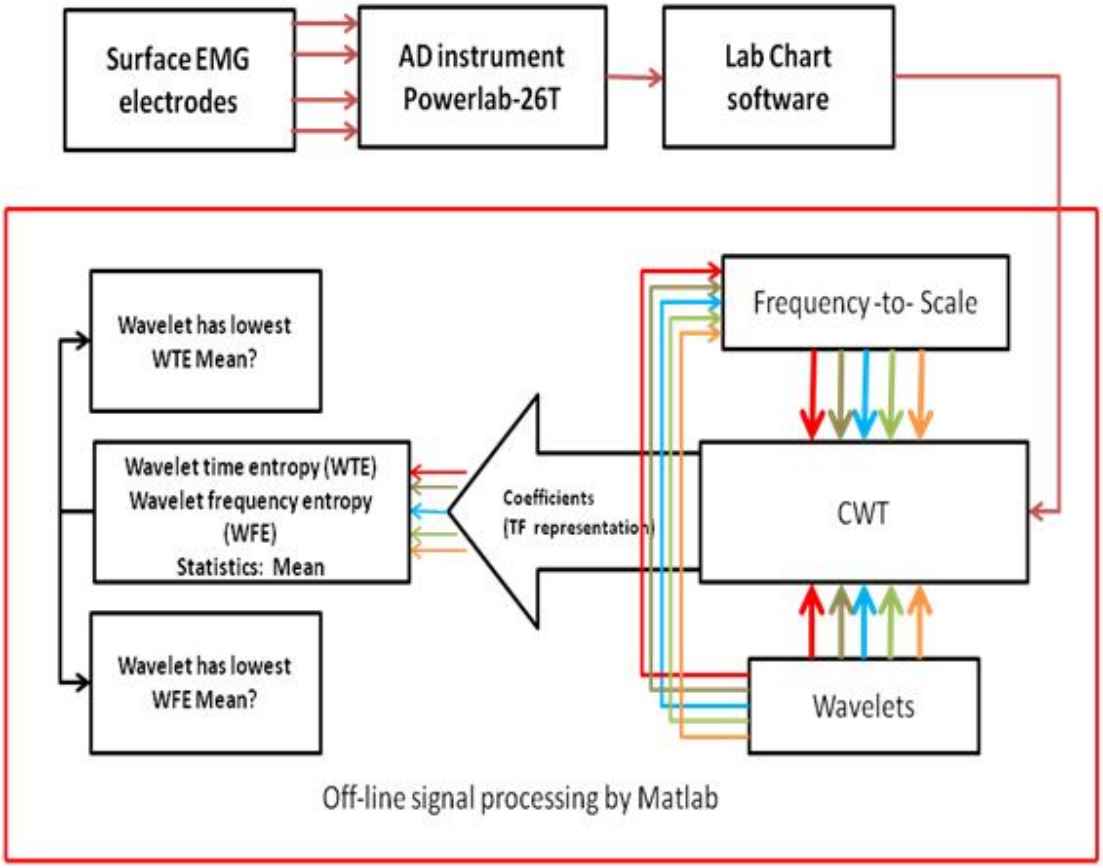

Figure 26: Methodology of analysis sEMG using CWT, WTE and WFE

3.1 Experiment Setup

To prove the hypothesis of utilizing WTE and WFE in identifying certain elements in human muscle EMG signals, experiments were conducted at the Sport and Health Exercise Department, Massey University, Albany Campus. The experiment apparatus includes AD instrument PowerLab, a force dynamometer, sEMG electrodes and skin cleaning swaps for a cleaner signal acquiring, as illustrated in figure 27.

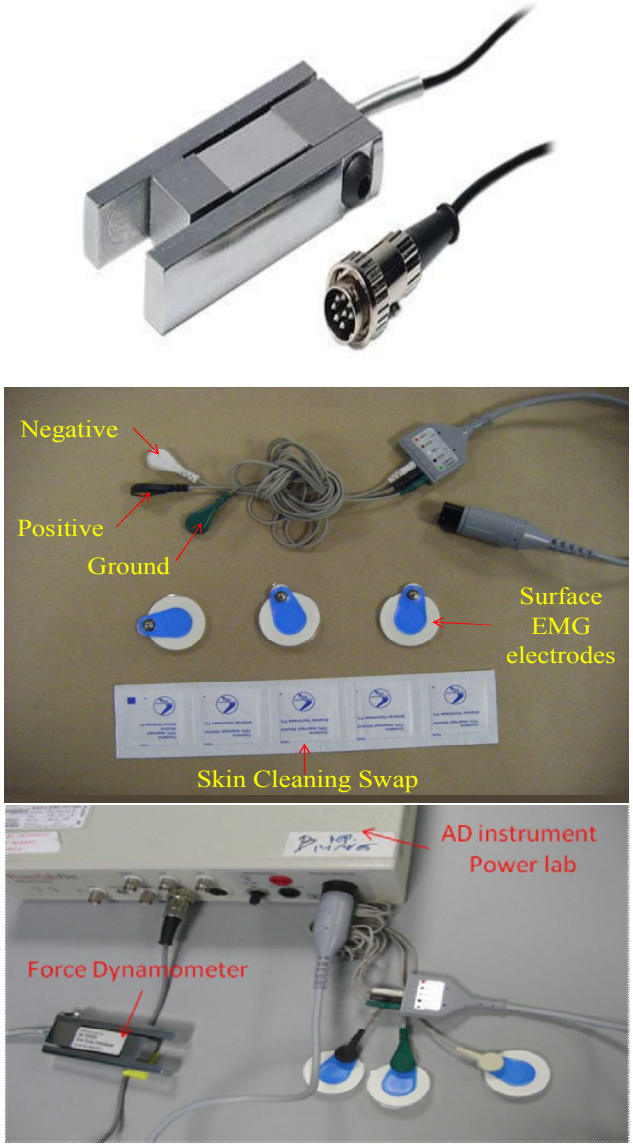

Figure 27: Devices and apparatus used in the experiment.

3.2 Experiment Measurements

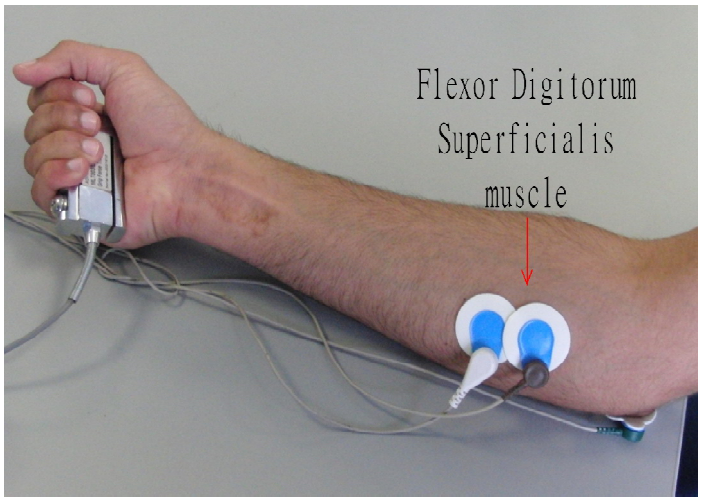

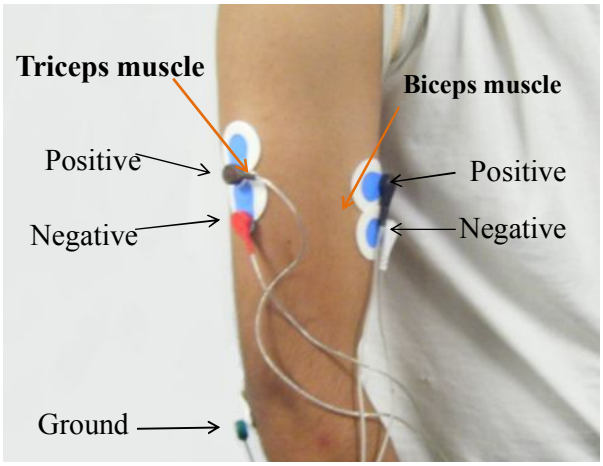

Figure 28: Placement of sEMG electrodes on muscles.

As shown in figure 28, the sEMG electrodes were placed on the forearm locations to detect EMG signals generated by the biceps, triceps and flexor digitorum superficialis (FDS) muscle. To provide a common reference, the patient shown in figure 28 is instructed to hold on to the force dynamometer which provides quantitative measures for muscle contractions to calibrate the corresponding sEMG measurements. With a sampling rate of 1000 samples per second, the output from the force dynamometer normalized with respect to the maximum muscle contraction is shown in figure 30. From the measurements, it is clear that consistent measures

can be much easier to achieve when the patient is asked to perform a contraction less than 60%. The inconsistent, or nonlinear, measures at high contraction rates are biologically due to the rapid engagement of motor units with emission on more electrochemical impulses.

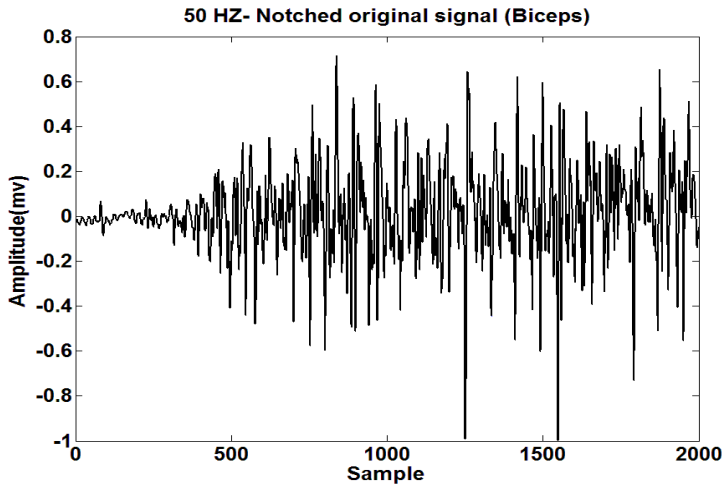

Figure 29: Typical biceps sEMG signal acquired by the experiment apparatus, sampling rate is 1k samples per second.

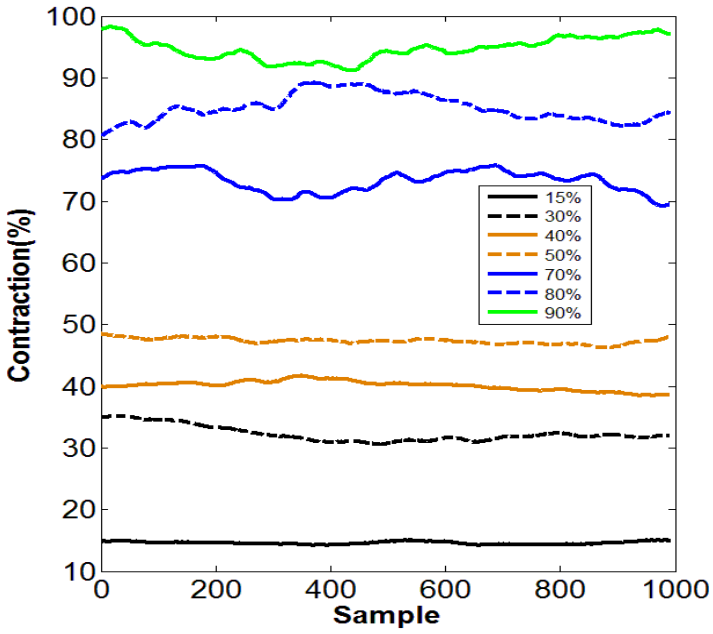

Figure 30: Measured percent contraction of FDS muscle over time.

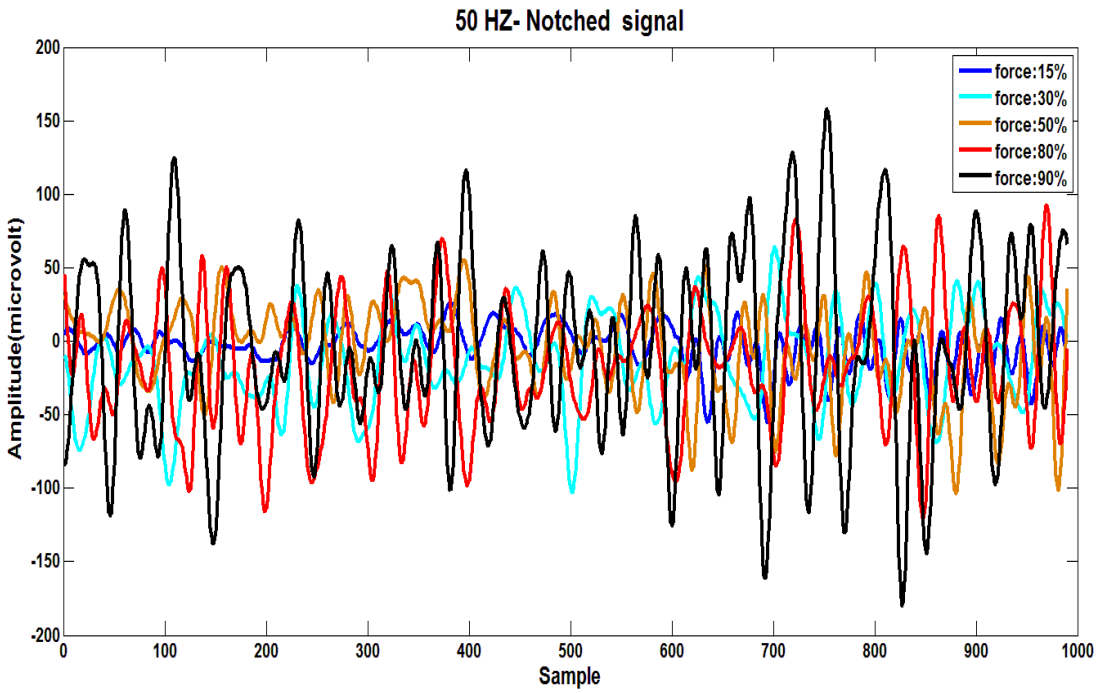

Figure 31: Measured sEMG vs. force of FDS muscle over time. Sampling rate is 1k samples per second

The sampling frequency in our present experiment for sEMG signal is 1k Hz. Following the work of Backus et al. (2010), our measured EMG signal is band-pass filtered between 1 Hz and 200 Hz along with 50 Hz notch filter to highlight bio-information provided by the muscles. This is accomplished electronically by the PowerLab chart software, and the biceps sEMG signal is illustrated in figure 29. Figure 31 shows the plot of measured sEMG vs. force of FDS muscle over time.

3.3 MATLAB code implementation

To achieve frequency scale conversion, equation 9 has been rearranged. The MATLAB code is:

```
   FS=1000;  % sampling frequency
 m=0;
For n=10:200  % desired frequency
```

```
m=m+1;  % index
scale_CMOR1(m)=(centfrq('cmor0.5-2')*FS)/(1*n);  % equivalent scale

end
```

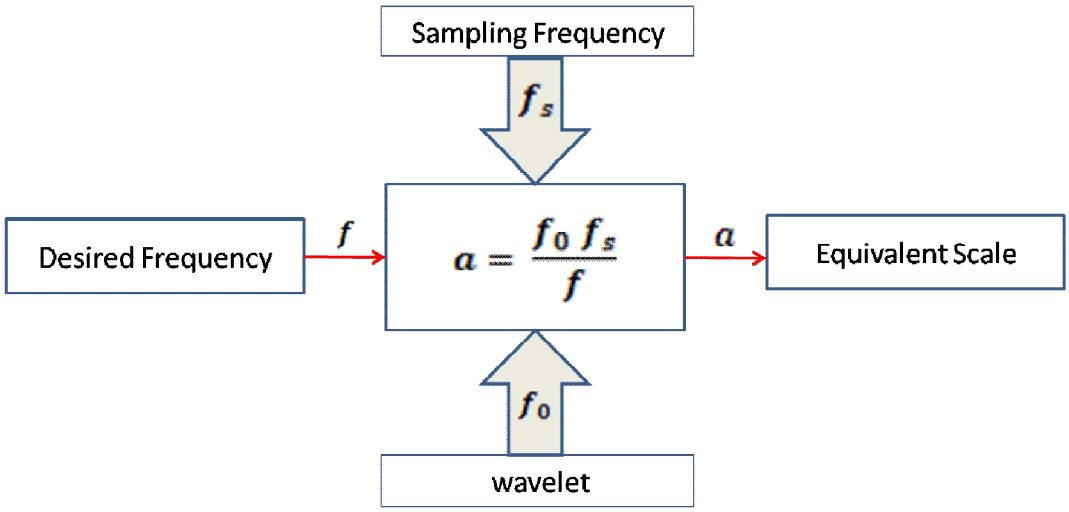

Figure 32: Frequency to scale conversion

The CWT of a particular wavelet has been implemented by the following code:

```
COEFS_1 = cwtext(y,scale_CMOR1,'cmor0.5-2');  % CWT code
COEFS_1_square=(abs(COEFS_1)).^2;  % CWT energy


B(1,:) = sum(COEFS_1_square);
C(1,:)= sum(transpose(COEFS_1_square));

R=MD(COEFS_1_square,B(1,:));
RR=MD1(COEFS_1_square,C(1,:));
[P,E(1,:)]=EC(R);
[PP,EE(1,:)]=EC1(RR);
```

A full code of implementation one of the wavelets (complex Morlet) is available in section one of the appendices.

Chapter 4: Results, Discussion and Analysis

The acquired EMG Data were analyzed off-line in Matlab. Several different wavelets have been utilized to analyze the raw sEMG signals. The mother wavelets in our present study include derivative of complex Gaussians (1-8), derivative of Gaussians (1-8), Daubecheies (1-15), Symlets (1-15), Coiflets (1-5), complex Morlet and complex Shannon. The last two mother wavelets are non-linear scaled and have different central frequencies, indexed by the numbers within the above parentheses, in which bandwidth ratios are implemented. The wavelets are scaled based on equation 9 to analyse the raw sEMG signals within the desired frequency range between 10 Hz and 200 Hz. The methodology in analysing the sEMG is best explained by the flowchart shown in figure 26 (refer to section three of appendices for the full results in this section).

4.1 Biceps muscle

4.1.1 Complex Morlet

The sEMG is analyzed by two types of complex Morlet wavelets, with ideas derived from nonlinear scaling. The types are:

Type1: constant- frequency bandwidth and variable central frequency.

Type2: variable- frequency bandwidth and constant central frequency.

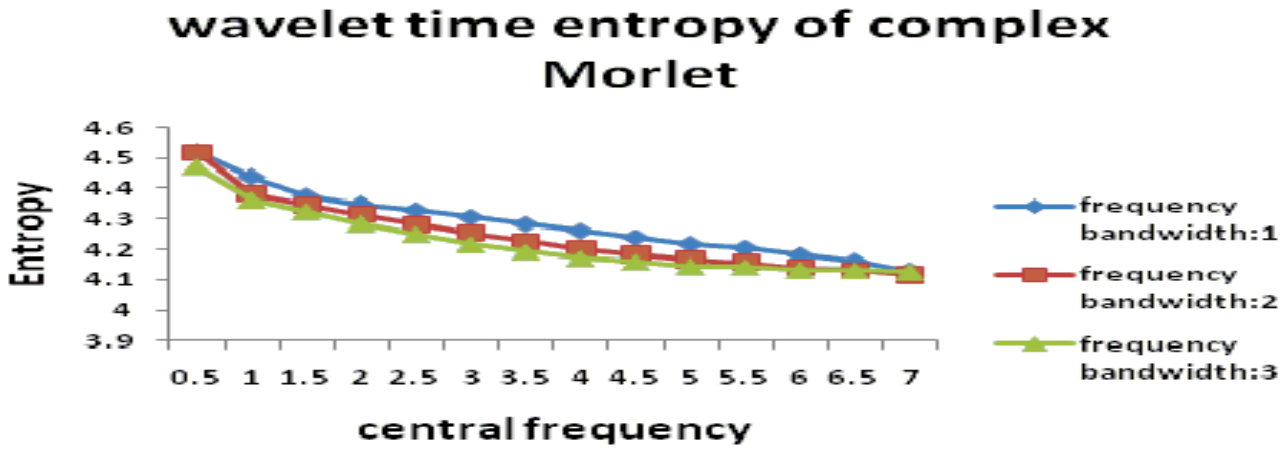

Figure 33: Wavelet time entropy of complex Morlet (constant frequency bandwidth, variable central frequency)

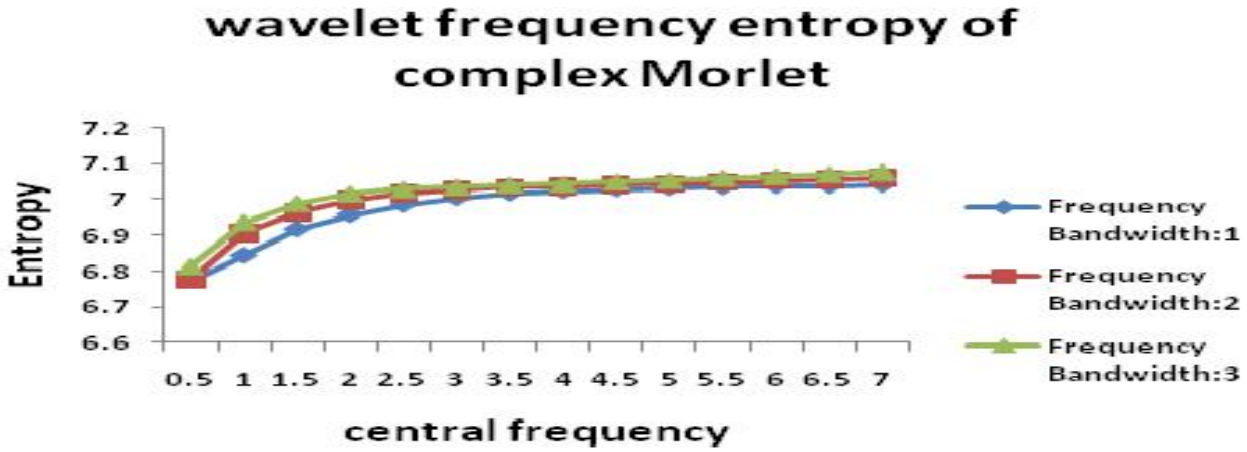

Figure 34: Wavelet frequency entropy of complex Morlet (constant frequency bandwidth, variable central frequency)

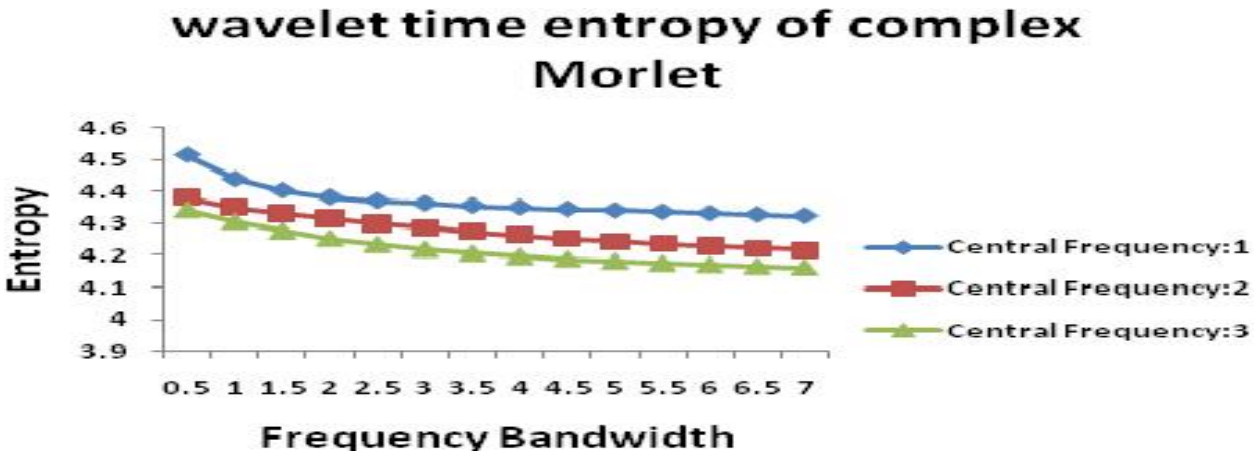

Figure 35: Wavelet time entropy of complex Morlet (variable frequency bandwidth, constant central frequency)

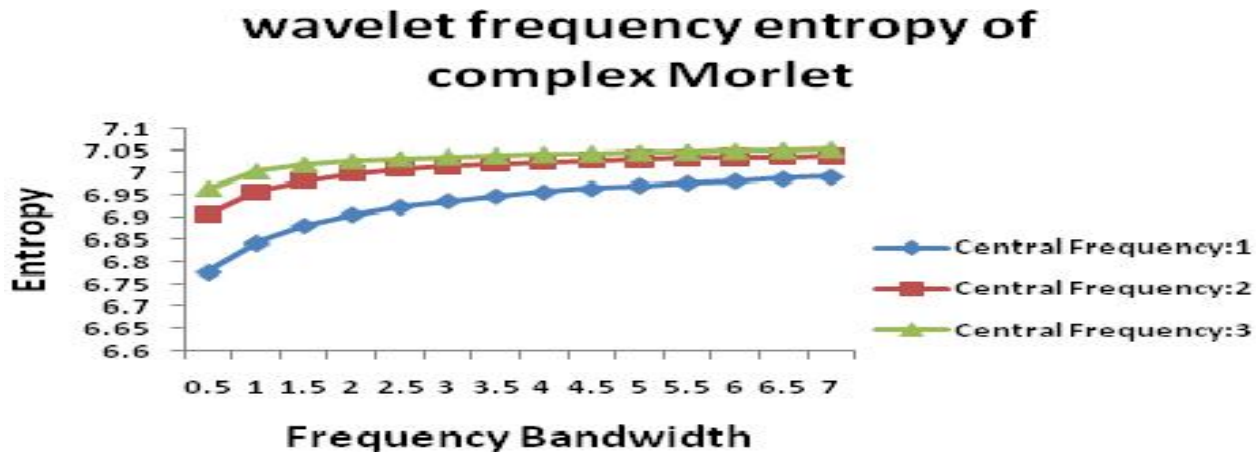

Figure 36: Wavelet time entropy of complex Morlet (variable frequency bandwidth, constant central frequency)

The Wavelet time entropy (WTE) of the complex Morlet decreases with the increase of central frequency for each constant frequency bandwidth, as shown in figure 33 (Type 1). The WTE results are found to be similar along with the increase of frequency bandwidth for a constant central frequency, as shown in figure 35 (Type 2).

In contrast, the Wavelet frequency entropy (WFE) of the complex Morlet behaves inversely; it increases with the increase of central frequency for each constant frequency bandwidth, as

shown in figure 34 (type 1). The WFE results are found to be similar along with the increase of frequency bandwidth for a constant central frequency, as shown in figure 36 (type 2).

In general, the values of WTE of complex Morlet are less than the values of WFE of complex Morlet.

4.1.2 Complex Shannon

The sEMG was analyzed using the same methodology for complex Morlet wavelets.

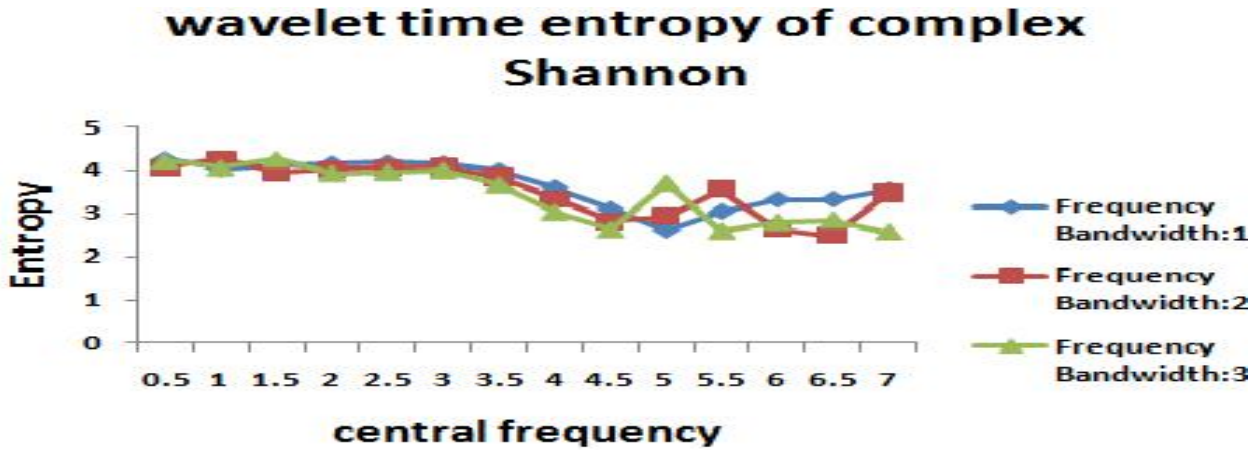

Figure 37: Wavelet time entropy of complex Shannon (constant frequency bandwidth, variable central frequency)

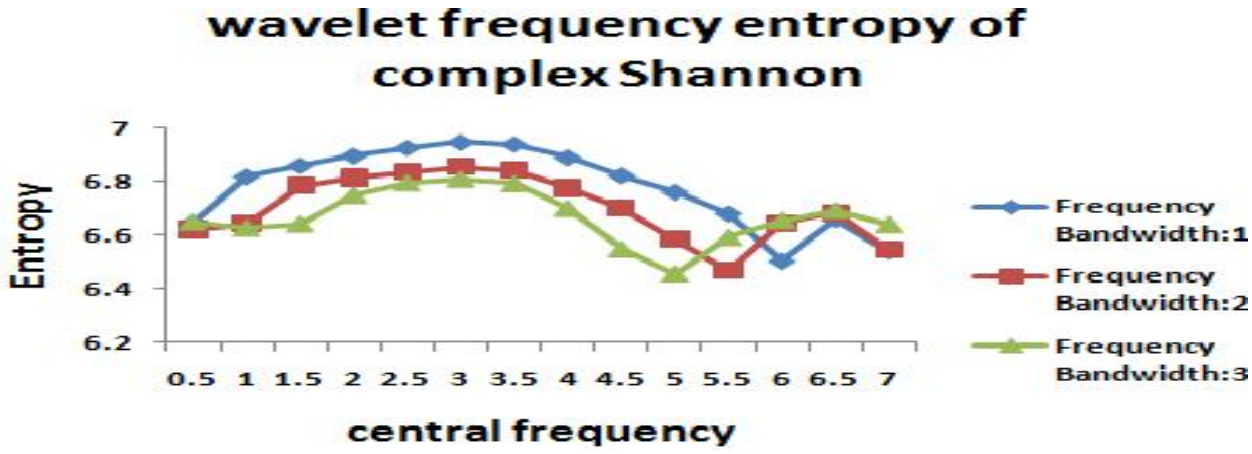

Figure 38: Wavelet frequency entropy of complex Shannon (constant frequency bandwidth, variable central frequency)

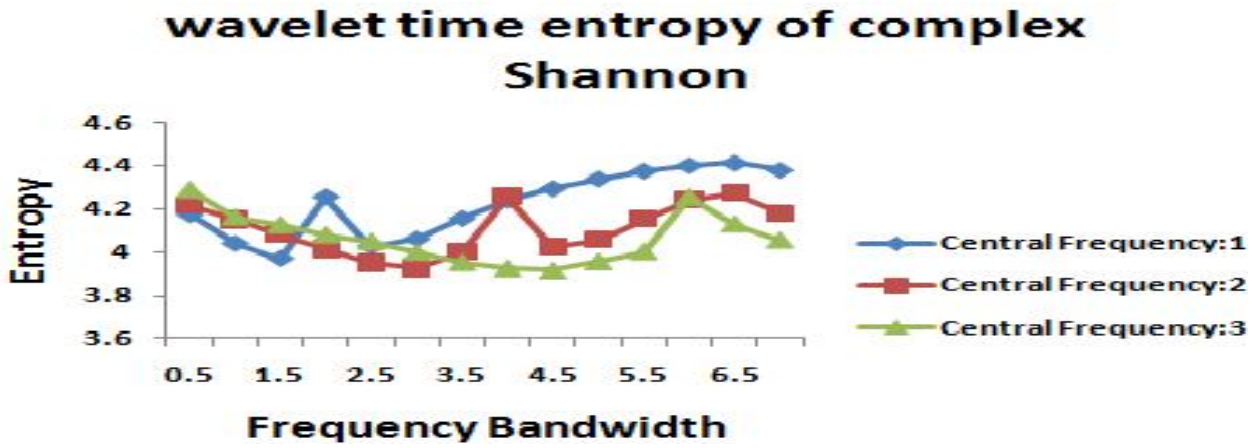

Figure 39: Wavelet time entropy of complex Shannon (variable frequency bandwidth, constant central frequency)

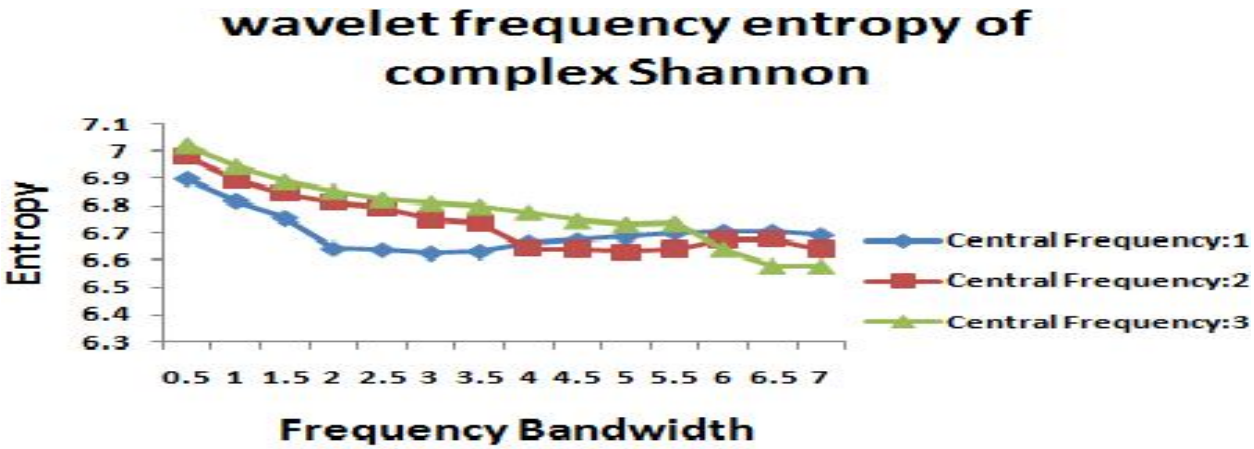

Figure 40: Wavelet frequency entropy of complex Shannon (variable frequency bandwidth, constant central frequency)

The Wavelet time entropy (WTE) and Wavelet frequency entropy (WFE) of complex Shannon have **non-consistent trends** with the increase of central frequency for a constant frequency bandwidth, as shown in figures 37 and 38. Similarly, they have **non-consistent trends** with the increase of frequency bandwidth for a constant central frequency, as shown in figures 39 and 40.

4.1.3 Symlets, Coiflets and Daubechies

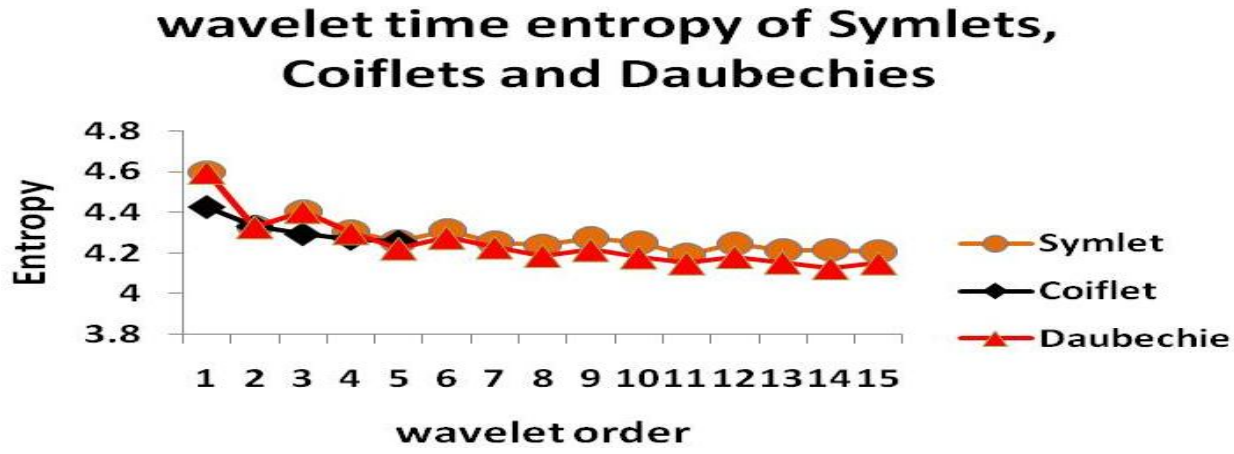

Figure 41: Wavelet time entropy of Symlets, Coiflets and Daubechies

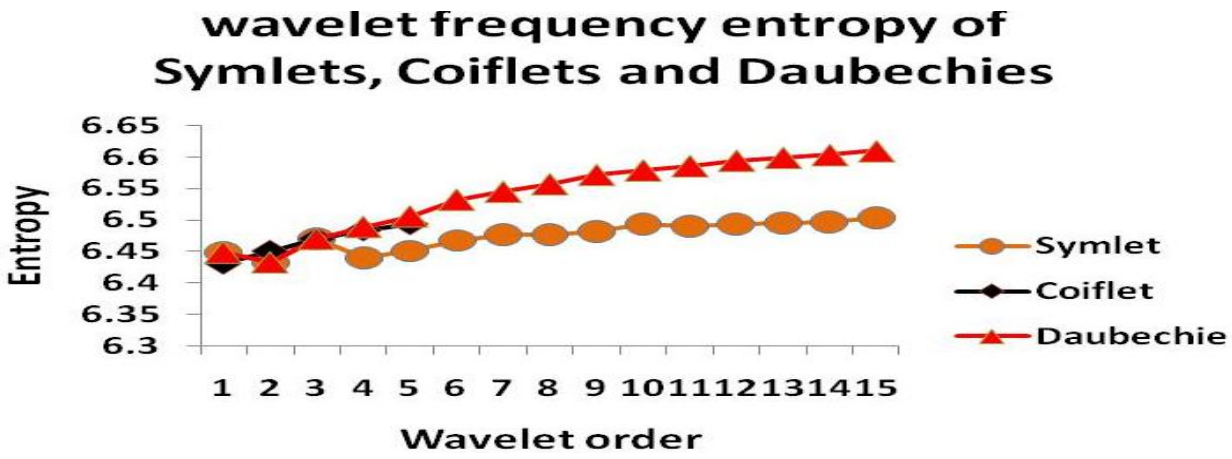

Figure 42: Wavelet frequency entropy of Symlets, Coiflets and Daubechies

Symlets, Coiflets and Daubechies have semi-linear behaviors of WTE and WFE are against the wavelet order. WTE of Symlets, Coiflets and Daubechies have a negative correlation with the wavelet order (Figure 41), while their WFEs have a positive correlation (Figure 42). Moreover, WTE values are less than WFE values. Daubechie-14 has the lowest WTE value.

4.1.4 Derivative of Gaussian (DOG) and Derivative of Complex Gaussian (DOCG)

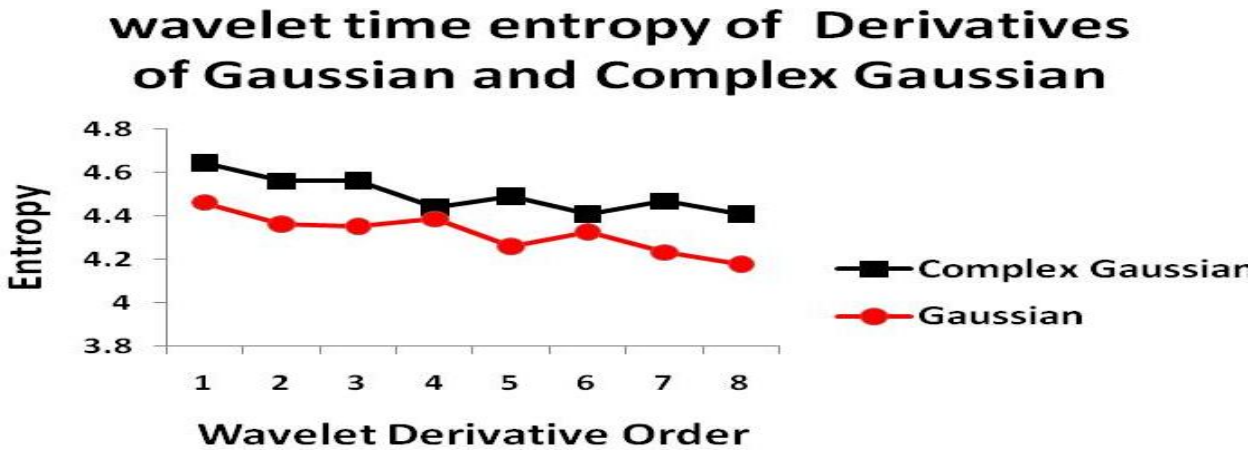

Figure 43: Wavelet time entropy of DOG and DOCG

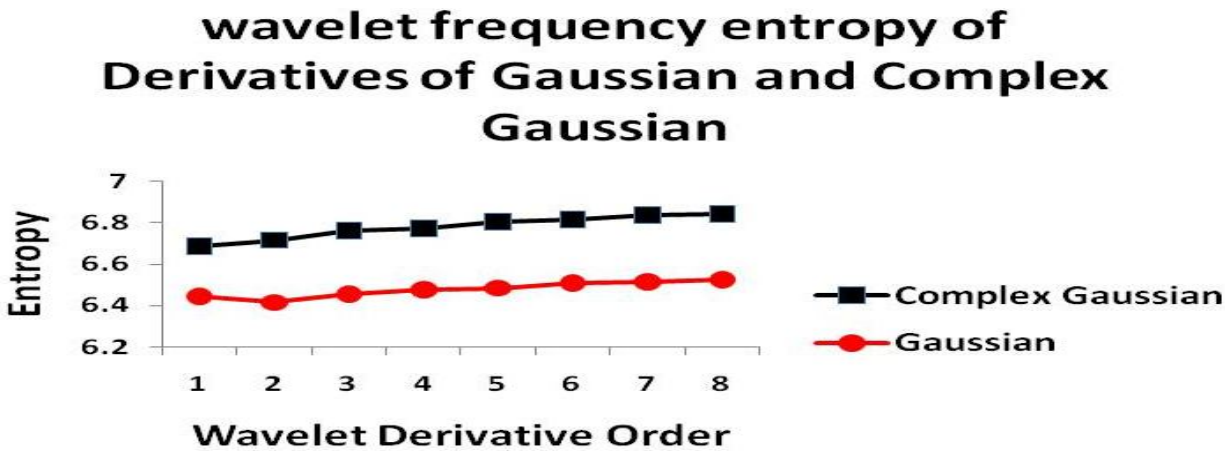

Figure 44: Wavelet frequency entropy of DOG and DOCG

The Wavelet time entropy (WTE) values of derivatives of Gaussian and derivatives of complex Gaussian have nearly negative-correlated linear trends with the derivative orders (Figure 43). However, their Wavelet frequency entropy values have nearly positive-correlated linear trends (Figure 44). WTE values are less than WFE values. Moreover, WTE values of Gaussian derivatives are less than WTE values of complex Gaussians derivatives. Therefore, Gaussian of 8^{th} derivative has the least WTE values.

4.1.5 Comparison of different lowest wavelet entropies

Figure 45 demonstrates that WTE values are less than WFE values. Moreover, complex Shannon wavelet has the lowest WTE value. The upper limit of complex Shannon is 2.8785 (2.4735+0.405), and is less than the values of the lower limits of WTE values of other wavelets, as shown in Table 4.

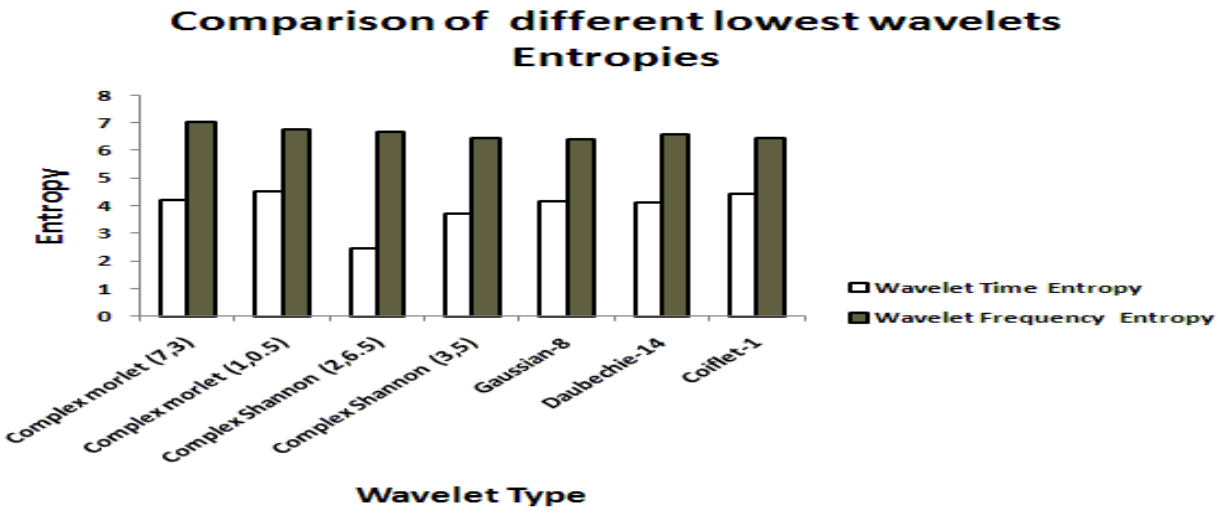

Figure 45: Comparisons of lowest wavelet entropy values of Biceps

Table 4: Comparison of lowest wavelet entropies

	WTE mean	WTE standard deviation	WFE mean	WFE standard deviation
Complex Morlet (7,3)	**4.2155**	**0.2639**	**7.0528**	**0.1346**
Complex Morlet (1,0.5)	**4.523**	**0.451**	**6.7716**	**0.1324**
Complex Shannon (2,6.5)	**2.4735**	**0.405**	**6.6823**	**0.1277**
Complex Shannon (3,5)	**3.7083**	**0.2391**	**6.4562**	**0.0894**
Gaussian-8	**4.1783**	**0.359**	**6.416**	**0.1272**
Daubechie-14	**4.1267**	**0.3053**	**6.6035**	**0.0962**
Coiflet-1	**4.4268**	**0.4737**	**6.4311**	**0.1478**

4.1.6 Data Consistency

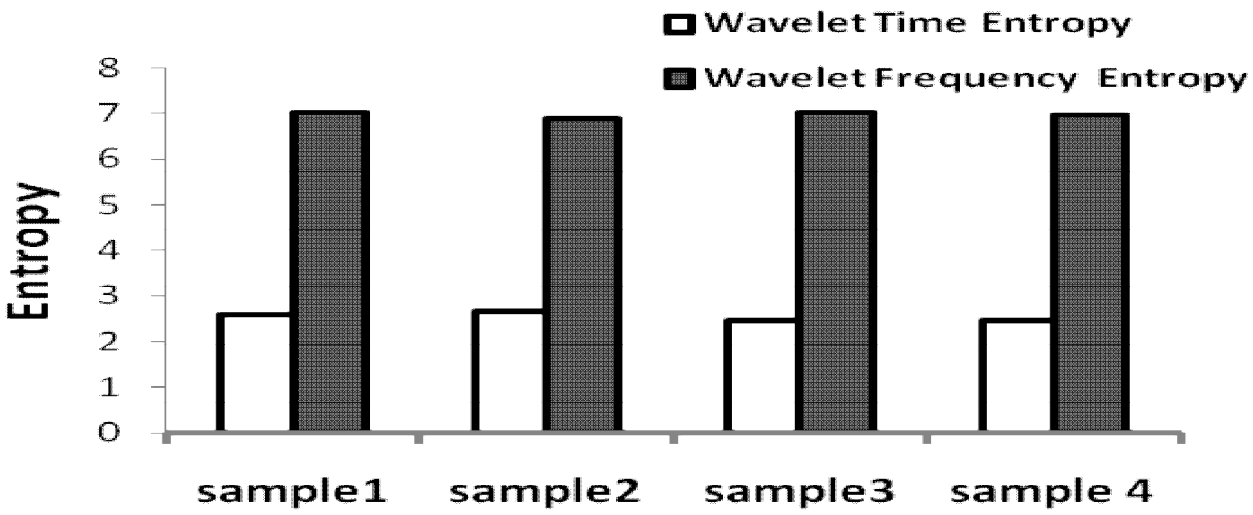

Figure 46: Entropy values of complex Shannon on biceps sEMG showing its consistency.

To investigate the consistency of the results, four samples of sEMG are obtained from the biceps. The samples have been analyzed using the proposed wavelets. Additionally, WTE values are lower than WFE values. The results are repeatable; this is shown over the four samples of Biceps sEMG in figure 46.

The consistency of the results indicates the robustness of the implemented methodology.

4.2 Flexor Digitorum Superficialis muscle

A study to explore the effects of different force contractions on WTE and WFE was proposed on the FDS muscle. Despite muscle contraction levels, the lowest entropy is located within the complex Shannon family WTE, as shown in figure 47.

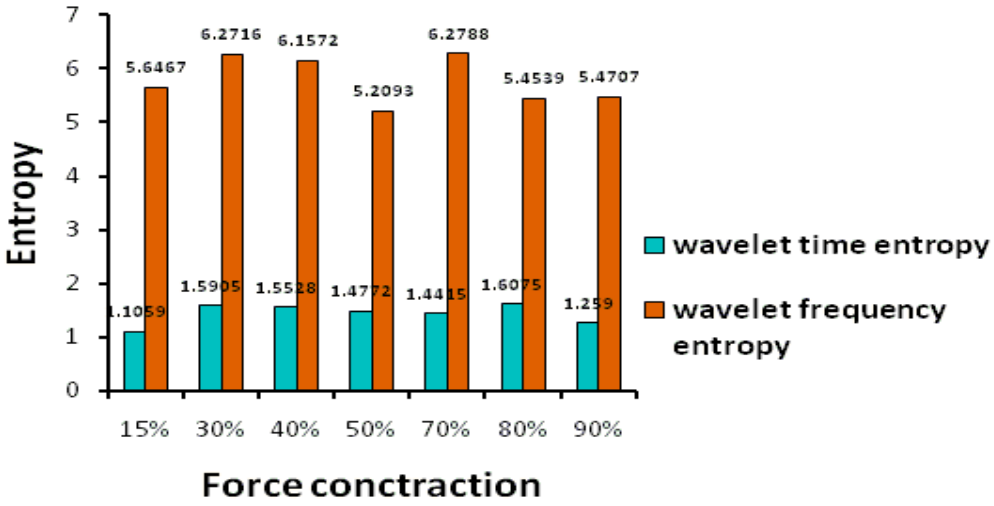

Figure 47: Lowest WTE &WFE values of Complex Shannon family along different force contraction.

This has qualitative engineering implications as it implies that the complex Shannon wavelet "maps" are very well correlated to the biceps and FDS sEMG time-domain signals. Based on equation 21, when the bandwidth frequency is given, one can easily calculate the corresponding muscle feature frequency with the entropy values.

It is noted that WTE values across different wavelet families are proportional to the muscle contraction, whereas the WFE does not follow the same trend. Furthermore, the standard deviation of complex Shannon wavelet WTE is small and does not step-in with the variance range of the second smaller WTE wavelet.

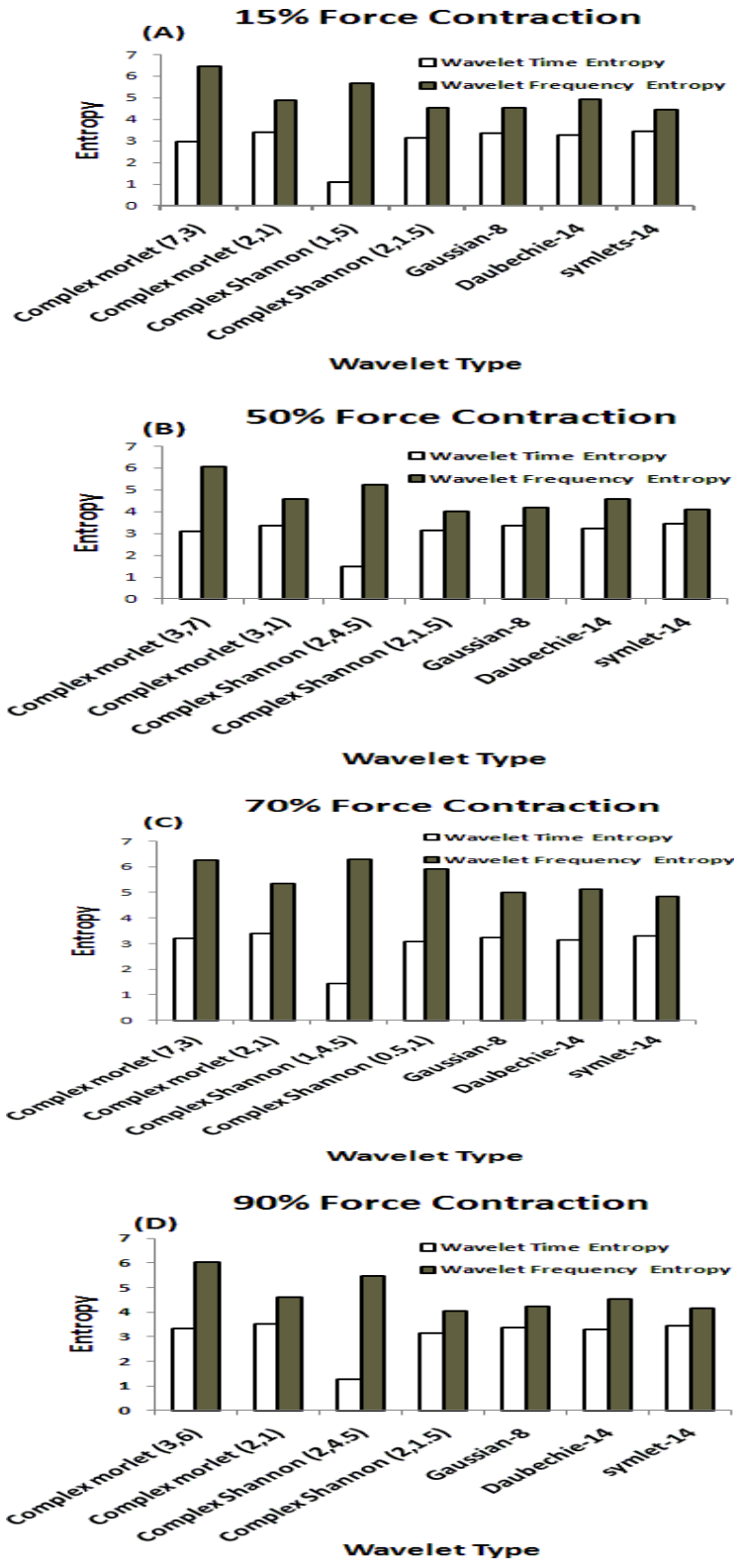

Figure 48: Comparison of different lowest wavelets entropies A: 15%, B: 50%, C: 70%, D: 90%

4.3 Consistency of results on a female subject

The same experiment methodology has been implemented on a different subject (female). The amplitude of obtained sEMG from Biceps muscle, as shown in figure 49, is between around -0.4 and 0.4 mv. The amplitude range is less than the Biceps sEMG, as shown in figure 29, which is within -0.7 and 0.7 mv. The second sample was taken from a male subject who had a larger muscle size compared to the female subject.

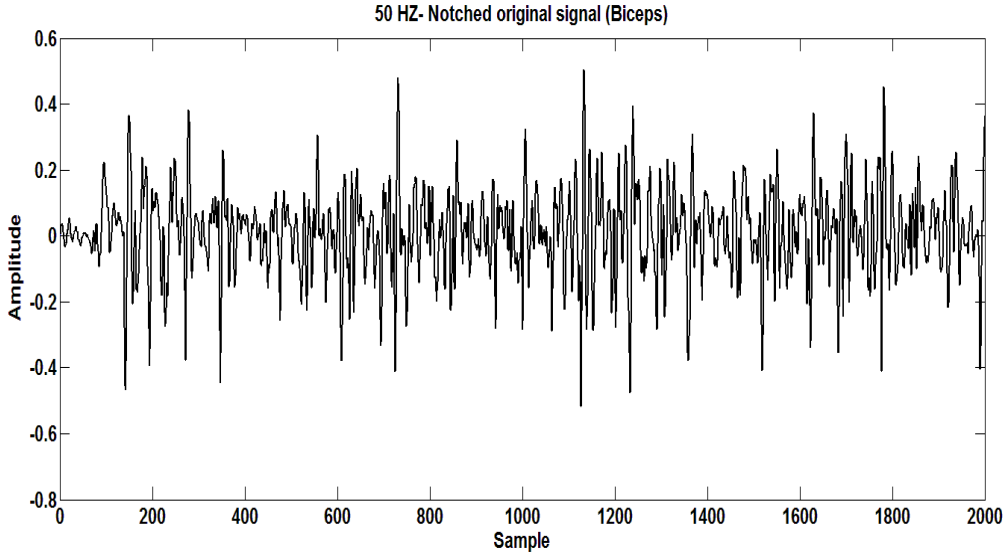

Figure 49: Typical biceps sEMG signal acquired by the experiment apparatus, sampling rate is 1k samples per second

However, a similar methodology of analysis had been carried out; complex Shannon family confirmed that it has the lowest WTE. The WTEs of complex Shannon are repeatable, as shown in Table 5.

Table 5: lowest WTE values (Complex Shannon Family)

Sample number	WTE
sample 1	**2.7028**
sample 2	**2.8903**
sample 3	**2.9291**
sample 4	**2.692**
sample 5	**2.9396**
sample 6	**2.9396**

Another experiment setup took place to measure Force versus sEMG signal. Due to the increase of the motor unit's activation with the increase of force contraction, it is clear that force measurements tend to be more inconsistent; especially when they are more than 60%, as shown in figure 50.

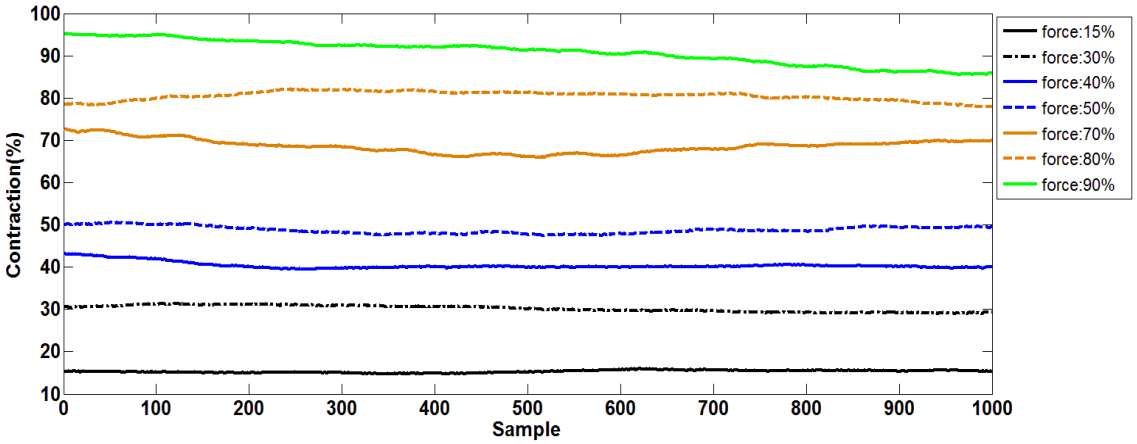

Figure 50: Measured percent contraction of FDS muscle over time (female subject)

The WTE values of the complex Shannon wavelet family (lowest compared to other wavelets types) over different force contractions are repeatable with a low standard deviation, as shown in figure 51. In addition, their WTE values are lower than WFE values.

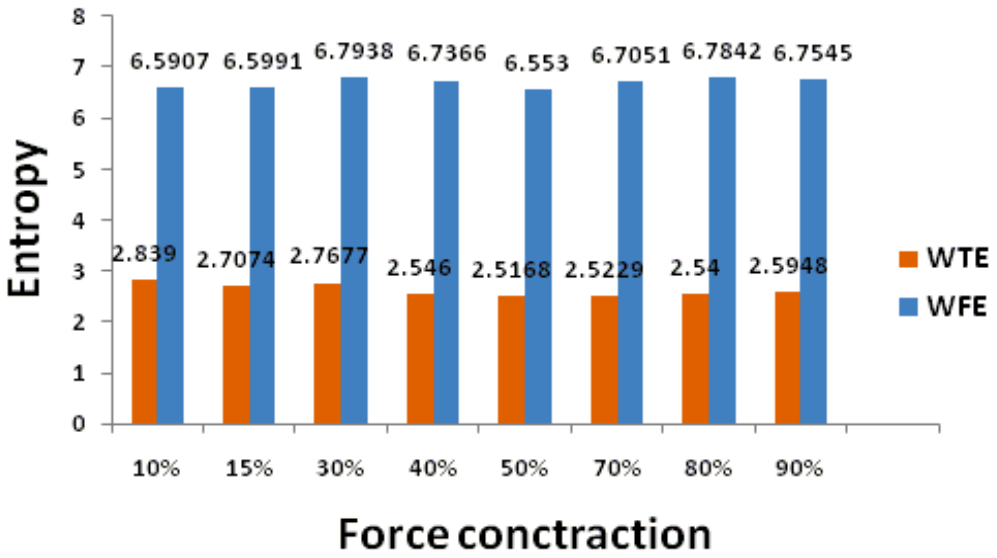

Figure 51: Lowest WTE &WFE values of Complex Shannon family along different force contraction (female).

4.4 Results Analysis

The findings on WTE and WFE could be explained under the concept "**Trade-off between time and frequency resolution via Heisenberg uncertainty principle**". It is known that the product of time resolution and frequency resolution equals constant. Hence, when time obtains higher resolution, the frequency resolution obtains lower resolution, and vice versa. This occurrence explains the decrease of WTE of DOG, DOCG, Symlets, Coiflets, Daubechies, complex Morlet and complex Shannon, in general, an increase of WFE of the same wavelets.

Complex Shannon wavelet has very good localization of energy in the frequency domain which is represented by a compact-supported rectangle, as shown in figure 18. However, it has poor or slow decay in the time domain. This possession explains the finding of lowest WTE through complex Shannon. WTE is a measurement of entropy on each sample along a range of scales. However, the average of WTEs is taken to obtain the mean WTE. Understanding the above two concepts gives a good reason why the complex Shannon wavelet has the lowest WTE.

A similar wavelet to the complex Shannon Wavelet is the Meyer wavelet; which has a nearly pulse-shaped frequency resolution and faster decay in the time domain. The thoughts that circulate in researchers' minds are possibilities of designing wavelets that contain very good frequency resolution and faster decay in the time domain in order to obtain better results of WTE and WFE, regardless of the effect of Heisenberg's uncertainty principle on WTE and WFE.

It is noticed that Daubechies, Symlets and Coiflets have negative trends of WTE along their orders. On the other hand, the vanishing moments of Daubechies wavelet is proportional with its order. A vanishing moment is described as the effect of the wavelet on different signals. A second order Daubechies wavelet has two vanishing moments which are zero mean and zero linear trends. When it is used to transform a data series, it removes mean and linear trends from the data series. A higher vanishing moment implies that more moments (quadratic, cubic, etc.) will be filtered out from the signal. Based on the negative trend of Daubechies wavelet and higher vanishing moments, the sEMG is represented by a complex polynomial equation.

Chapter 5: Conclusion, Constraints and Future Work

5.1 Conclusion

The research scope has covered two areas, neuromuscular systems and signal processing techniques. The integration of the two areas aimed at improving the information extraction of biological signals has been the focus of this research. Selection of the best bio-signal processing technique had been based on the comparison and refinement of properties of signal processing technique, being the Hilbert Huang Transform, Continuous Wavelet Transform and Short Time Fourier Transform, to meet the properties of surface electromyography signals as well as other conditions such as complexity of technique implementation, equipment availability and software availability. After careful idea rectification, the decision was on Continuous Wavelet Transform which was selected over Discrete Wavelet Transform due to its data redundancy. After that, the research aim had come to scrutinize the usefulness of applying Continuous Wavelet Transform in exploring surface electromyography signals of human muscles. Several identified wavelets have been applied in continuous wavelet transform to extract features from measured surface electromyography signals.

Entropy measurement has been adopted along continuous wavelet transform to identify the best similar wavelet to surface electromyography signals. The integrated wavelet entropy technique was developed into two parts; Wavelet frequency entropy and Wavelet time entropy.

Unlike Wavelet frequency entropy, it was illustrated that Wavelet time entropy indexes gave better certainty of continuous wavelet transform in identifying muscle signals. Among the proposed wavelets, complex Shannon wavelet was discovered to provide the lowest Wavelet time entropy which qualitatively implies higher “certainty” in identifying the muscle actions and

detection of signal contents. These two results have engineering implications in bio-medical and bio-robotics applications.

One of the weaknesses of the wavelet theory is that central frequency is dependent on the mother wavelet. This shortcoming was solved by rearranging the pseudo frequency equation to analyze the signal within the desired frequency range.

5.2 Constraints

5.2.1 Complexity of the neuromuscular system and lacking experience

Each muscle composes of a few to hundreds of different motor units from smallest to largest thresholds. The motor unit requirement, based on "Henneman's Size Principle" along with unknown distribution of motor units on the muscle, makes it hard to analyze the recorded signal. The recorded EMG signal is within the disk surface of the electrode. Therefore, not all the motor units' firing rates are recorded. By changing the position of the electrode along the muscle, it is possible to get different EMG signals.

5.2.2 Off-line processing vs. on-line processing

After conducting a number of experiments using off-line processing, it has been noted that using an on-line processing method would be more appropriate, and allows an instant viewing of the signal processing and data analysis. Another advantage of using on-line processing is that data can be collected and processed within the same software, ensuring that the settings are consistent between the collecting stage and the processing stage of data. On the other hand, when using an off-line processing method, there is always the risk of failing to set the required components from software to the other (e.g., from AD instrument during the data collection to MATLAB for the processing stage).

5.2.3 Software functions

The unavailability of inverse Continuous Wavelet Transforms function will not enable the reconstruction of the signal within the desired scales (desired frequencies) from the time-frequency representation. Therefore, the amount of noise reduction cannot be specified as long as the signal is not reconstructed. In addition, SNR would not be implemented to investigate the quality of filtered signals.

5.3 Future Work

The history of wavelet theory is not long, having been around for only three decades, but it has been gaining an excellent reputation in non-stationary signal filtering and feature extraction. Adopting and developing other wavelets, such as Paul, gamma and beta wavelets, acquired from different areas (like speech and image processing) are a key option of further study. Along with this, compromising two wavelets that have good and different properties on both the time and frequency domains (such as complex Shannon and Myer wavelet) to produce a modified wavelet is the key for further development in wavelet signal processing of neuromuscular systems.

In addition, another idea that came up was the possibility of implementing zero crossing algorithms to find the frequency and compare the results with Energy-frequency Distribution of each wavelet, in order to confirm the proposed method. However, the non-stationary frequency feature of EMG signals and running out of time got in the way of implementation this. There has been the proposed idea of “Zero-Crossing Intervals of Gaussian Processes” (Rainal, 2003). The integration of zero crossing algorithms with wavelet theory can be another future development key.

This research has provided me with a line of credit, starting with obtaining experience in neuromuscular systems, to understanding the concept of non-stationary signal filtering and processing. Surfing through the math sea of wavelet theory has expanded and supported my ability of designing a wavelet according to the requirements.

Reference

Addison, P. (2002). *The Illustrated Wavelet Transform Handbook*. New York, USA, and London, UK: Taylor & Francis Group.

AD Instruments. (2010). *EMG.* AD Instrument Inc. Retrieved May 2010 from http://www.adinstruments.com/solutions/research/EMG/

Agarwal, V., and Tsoukalas, L..H. (2007). Denoising electrical signal via Empirical Mode Decomposition. *2007 IREP Symposium- Bulk Power System Dynamics and Control – VIII. Revitalizing Operational Reliability (IREP)*.

Alsberg, B.K., Kell, D.B., and Woodward, A.M. (1997). An introduction to wavelet transforms for chemometricians. A time-frequency approach. *Chemom. Intell. Lab. Syst*.

Backus, S.I., Tomlinson, D.P., Vanadurongwan, B., Lenhoff, M.W., Cordasco, F. A., Chehab, E.L., Adler, R.S., Henn, R.F. and . Hillstrom, H.J., (2010). "A spectral analysis of rotator cuff musculature electromyographic activity: Surface and indwelling. *HSS Journal.*

Castellini, C., Fiorilla, A.E., and Sandini, G. (2009). Multi-subject/daily-life activity EMG-based control of mechanical hands. *J. NeuroEngineering and Rehabilitation.* Vol. 6(41).

Chen, F., and Zhang, Y.T. (2005). A new implementation of discrete bionic wavelet transform: Adaptive tiling. *Digital Signal Processing*. Vol. 16(3). Pp. 233-246.

Costa, H.C.A., and de Matos, M.C. (2008). Measuring time between peaks in helicopter classification using Continuous Wavelet Transform. *IEEE Radar Conference.*

Daubechies, I. (1991). Ten lectures on wavelets. *CBMS- NSF Series in Applied Mathematics (SIAM)*.

De Luca, C.J. (2008). Imaging *the Behavior of Motor Units by Decomposition of the EMG Signal*. Boston, USA: Delsys inc.

De Luca, C.J. (2008). *Practicum on the use of surface EMG signals in movement science.*Vol. 1(5). Boston, USA: Delsys inc.

De Luca, C.J., Adam, A., Wotiz, R., Gilmore, L.D., and Nawab, S.H. (2006). Decomposition of surface EMG signals. *J. Neurophysiol*.

Enoka, R.M., and Stuart, D.G. (1984). Henneman's 'size principle': current issues. *Trends in Neurosciences.* Vol. 7(24).

Feng, Z.. Ding, X., and Jiang, Y. (2010). Pitch Period estimation of voice signal based on EEMD and Hilbert Transform. *2nd International Asia Conference on Informatics in Control, Automation and Robotics (CAR).*

Goreczny, A.J. (1995). *Handbook of health and rehabilitation psychology.* New York: Plenum Press.

Grigoryan, A.M. (2005). Fourier Transform representation by frequency-time wavelets. *IEEE Transactions on Signal Processing.* Vol. 53(7).

Han, S., Sun, B., Wu, C., and He, L.. (2009). Dynamic characteristic analysis of power system low frequency oscillation using Hilbert-Huang transform. *Power Systems Conference and Exposition.*

Hof, A.L. (1984). EMG and muscle force: an introduction. *Human Movement Science*. Vol. 3(1-2).

Huang, N. E., and Shen, S.S.P. (2005). Hilbert-Huang transform and its applications, Singapore, Hackensack, London: World Scientific Publishing ltd.

Ismail, A.R., and Asfour, S.S. (1998). Continuous wavelet transforms application to EMG signals during human gait. *Conference Record of the Thirty-Second Asilomar Conference on Signals, Systems & Computers.* Vol. 1. Pp. 325 – 329.

Jiang, N., Parker, P. A., and Englehart K. B. (2007). Extracting neural drives from surface EMG: A generative model and simulation studies. *Proceedings of the 29th annual international conference of the IEEE EMBS in engineering in medicine and biology society*.

Kaiser, G. (1995). A friendly guide to wavelets. Boston: Birkhäuser.

Kiymik, M., Güler, I., Dizibüyük, A., and Akin, M. (2004). Comparison of STFT and wavelet transform methods in determining epileptic seizure activity in EEG signals for real-time application. *Computers in Biology and Medicine*. Vol.35 (7). Pp.603-616.

Lau, K.M., and Wcng, H.Y. (1995). Climate signal detection using wavelet transform: how to make a time series sing. *Bulletin of the American Meteo.* 76(12): 2391.

Lee, K.W., He, T., Ilhan, H.T., Linscott, I., and Olgin, J.E. (2005). Feature extraction of the atrial fibrillation signal using the continuous wavelet transform. *26th Annual International Conference of the IEEE Engineering in Medicine and Biology Society.* Pp. 275 – 278.

Lee, J.J., Lee, S.M., Kim, I.Y., Min, H.K., and Hong, S.H. (1999). Comparison between short time Fourier and wavelet transform for feature extraction of heart sound. *10 Conference (TENCON 99) proceedings of the IEEE region*.

Liu, Z., Liu, C., Liu, B., Lv, Y., Lei, Y., and Yu, M. (2005). Self spectrum window method in wigner-ville distribution. *27th Annual International Conference of the Engineering in Medicine and Biology Society (IEEE-EMBS 2005)*.

Mallat, S.G. (1998). A wavelet tour of signal processing, San Diego, London, Boston, New York, Sydney, Tokyo, and Toronto: Academic Press.

Mishra, A.K., özger, M., and Singh, V.P. (2009). An entropy-based investigation into the variability of precipitation. *J. of Hydrology.* Vol. 370(1-4). Pp. 139–154.

Nurco, D.J., Conklin, D.E., and Shapiro, N.S., (2009). Motor unit recruitment strategies during deep muscle pain. *Word Press.*

Norman, C. F.T., and Lai L..L., (2007). Wavelet-Based algorithm for signal analysis. *EURASIP Journal on Applied Signal Processing*.

Peng, Z.K., Tse, P.W., and Chu, F.L.. (2005). An improved Hilbert–Huang transform and its application in vibration signal analysis. *J. Sound and Vibration*. Vol. 286(1-2).

Peng Z.K., Tse, P. W., Chu, F.L.. (2005). A comparison study of improved Hilbert–Huang transform and wavelet transform: Application to fault diagnosis for rolling bearing. *Mechanical Systems and Signal Processing.* Vol. 19(5).

Rafiee, J., Schoen, M.P., Prause, N., Urfer, A., and Rafiee, A.M. (2009). A comparison of forearm EMG and psychophysical EEG signals using statistical signal processing. *2nd International Conference on Computer, Control and Communication*.

Rainal, A. (2003). Zero-crossing intervals of Gaussian processes. *IRE Transactions on Information Theory*. Vol 8(6).

Rajagopalan, V., and Ray, A. (2006). Symbolic time series analysis via wavelet-based partitioning. *Signal Processing.* Vol. 86(11), Pp. 3309-3320.

Scheper, R.A., and Teolis, A. (2003). Cramer-Rao Bounds for wavelet Transform-Based instantaneous frequency estimates. *IEEE Transaction on Signal Processing.*

Seiler, S. (n.d). *Basic skeletal muscle physiology - The motor unit*. Retrieved 24 April 2010 from http://www.time-to-run.com/physiology/skeletal-muscle/motor.htm

Sejdic, E., Djurovic, I., and Jiang, J. (2009). Time-Frequency feature representation using energy concentration: An overview of recent advances. *Digital Signal Processing (Elsevier)*. Vol. 19, issue 1. Pp. 153-183.

Stokes, I.A.F., Henry, S.M., and Single, R.M. (2003). Surface EMG electrodes do not accurately record from lumbar multifidus muscles. *J. Clinical Biomechanics*. Vol. 18(1).

Teolis, A. (1998). Computational signal processing with wavelets. Boston: Birkhäuser.

Top end sports. *Sports medicine. Fast and slow twitch muscle fibres.* Retrieved 25 April 2010 from http://www.topendsports.com/medicine/physiology-muscles.htm

Torrence, C., and Compo, G.P. (1998). A practical guide to wavelet analysis. *Bull. Am. Meteorol*. Soc. 79. Pp 61–78.

Toxin. (2009). *Motor unit recruitment strategies during deep muscle pain.* Retrieved 1 May 2010 from http://natchem.wordpress.com/

Von Tscharner, V. (2000). Intensity analysis in time–frequency space of surface myoelectric signals by wavelets of specified resolution. *J. Electromyogr. Kinesiol.* Vol. 10. Pp. 433–445.

Wei, L., and Pei-Wen, Q. (2009). Optimal scale wavelet transform for the identification of weak ultrasonic signals. *J. Measurements.* Vol. 42(1).

Wen, k.L., and Qiang, Z. (2009). Deconvolutive Short-Time Fourier Transform Spectrogram. *IEEE Signal Processing Letters.* Vol. 16. Pp. 576 – 579.

Winter, D.A. (2009). *Biomechanics and motor control of human movement.* Hoboken, NJ: USA.

Xie, X.P., and Ding, X.H. (2009). Gene Expression Pattern Extraction based on wavelet analysis. *International Conference on Information and Automation.* Pp. 1274 – 1278.

Yang, X., and Tang, J.T. (2008). Hilbert-Huang Transform and Wavelet Transform for ECG detection*, 4th International Conference on Wireless Communications, Networking and Mobile Computing (WiCOM '08.).*

Yan, R., and Gao, R.X. (2006). Hilbert–Huang Transform-Based vibration signal analysis for machine health monitoring. *IEEE Transactions on Instrumentation and Measurement*. Vol. 55(6).

Yao, J., and Zhang, Y.T. (2001). Bionic Wavelet Transform: A new time–frequency method based on an auditory model. *IEEE Transactions on Biomedical Engineering*. Vol. 48(8).

Yu, D., Cheng, J., and Yang, Y. (2005). Application of EMD method and Hilbert spectrum to the fault diagnosis of roller bearings. *Mechanical Systems and Signal Processing.* Vol. 19 (2).

Zhengyou, H.X.C., and Qingquan, Q. (2007).A Study of wavelet entropy measure and definition and its application for fault feature pick-up and classification. *J. of Electron.* Vol. 24(5).

Zheng-You, H., Xiaoqing, C., and Guoming, L.. (2006). Wavelet entropy measure definition and its application for transmission line fault detection and identification. *Proceedings of the 2006 International Conference on Power System Technology*. Pp. 1–6.

Appendices

Section One: Implementation code

The following program is an example of CWT implementation of complex Morlet

1. Main program

```
clear all;
close all;


%load RS.mat
load BI_TR.mat;
%RS=BI_1;
RS=BI_2;
t=1:length(RS);
plot(t,RS,'b');
%figure
hold on

y=RS;
plot(t,y,'r');
title('50 HZ- Notched original signal');
xlabel('Sample');
Ylabel('Amplitude');

 % Frequency to scale conversion
%-------------------------------------------------------
FS=1000;
  m=0;
for n=10:200
  m=m+1;
            scale_CMOR1(m)=(centfrq('cmor0.5-2')*FS)/(1*n);
            scale_CMOR2(m)=(centfrq('cmor1-2')*FS)/(1*n);
            scale_CMOR3(m)=(centfrq('cmor1.5-2')*FS)/(1*n);
            scale_CMOR4(m)=(centfrq('cmor2-2')*FS)/(1*n);
            scale_CMOR5(m)=(centfrq('cmor2.5-2')*FS)/(1*n);
            scale_CMOR6(m)=(centfrq('cmor3-2')*FS)/(1*n);
            scale_CMOR7(m)=(centfrq('cmor3.5-2')*FS)/(1*n);
            scale_CMOR8(m)=(centfrq('cmor4-2')*FS)/(1*n);
            scale_CMOR9(m)=(centfrq('cmor4.5-2')*FS)/(1*n);
            scale_CMOR10(m)=(centfrq('cmor5-2')*FS)/(1*n);
            scale_CMOR11(m)=(centfrq('cmor5.5-2')*FS)/(1*n);
            scale_CMOR12(m)=(centfrq('cmor6-2')*FS)/(1*n);
```

```
        scale_CMOR13(m)=(centfrq('cmor6.5-2')*FS)/(1*n);
        scale_CMOR14(m)=(centfrq('cmor7-2')*FS)/(1*n);


end
 %-------------------------------------------------------
COEFS_1 = cwtext(y,scale_CMOR1,'cmor0.5-2');
COEFS_1_square=(abs(COEFS_1)).^2;

COEFS_2 = cwtext(y,scale_CMOR2,'cmor1-2');
COEFS_2_square=(abs(COEFS_2)).^2;

COEFS_3 = cwtext(y,scale_CMOR3,'cmor1.5-2');
COEFS_3_square=(abs(COEFS_3)).^2;

COEFS_4 = cwtext(y,scale_CMOR4,'cmor2-2');
COEFS_4_square=(abs(COEFS_4)).^2;

COEFS_5 = cwtext(y,scale_CMOR5,'cmor2.5-2');
COEFS_5_square=(abs(COEFS_5)).^2;

COEFS_6 = cwtext(y,scale_CMOR6,'cmor3-2');
COEFS_6_square=(abs(COEFS_6)).^2;

COEFS_7 = cwtext(y,scale_CMOR7,'cmor3.5-2');
COEFS_7_square=(abs(COEFS_7)).^2;

COEFS_8 = cwtext(y,scale_CMOR8,'cmor4-2');
COEFS_8_square=(abs(COEFS_8)).^2;

COEFS_9 = cwtext(y,scale_CMOR9,'cmor4.5-2');
COEFS_9_square=(abs(COEFS_9)).^2;

COEFS_10 = cwtext(y,scale_CMOR10,'cmor5-2');
COEFS_10_square=(abs(COEFS_10)).^2;

COEFS_11 = cwtext(y,scale_CMOR11,'cmor5.5-2');
COEFS_11_square=(abs(COEFS_11)).^2;

COEFS_12 = cwtext(y,scale_CMOR12,'cmor6-2');
COEFS_12_square=(abs(COEFS_12)).^2;

COEFS_13 = cwtext(y,scale_CMOR13,'cmor6.5-2');
COEFS_13_square=(abs(COEFS_13)).^2;

COEFS_14 = cwtext(y,scale_CMOR14,'cmor7-2');
COEFS_14_square=(abs(COEFS_14)).^2;

%---------------------------------------
```

```
B(1,:) = sum(COEFS_1_square);
C(1,:)= sum(transpose(COEFS_1_square));
R=MD(COEFS_1_square,B(1,:));
RR=MD1(COEFS_1_square,C(1,:));
[P,E(1,:)]=EC(R);
[PP,EE(1,:)]=EC1(RR);
%---------------------------------------
B(2,:) = sum(COEFS_2_square);
C(2,:)= sum(transpose(COEFS_2_square));
R=MD(COEFS_2_square,B(2,:));
RR=MD1(COEFS_2_square,C(2,:));
[P,E(2,:)]=EC(R);
[PP,EE(2,:)]=EC1(RR);
%---------------------------------------

B(3,:) = sum(COEFS_3_square);
C(3,:)= sum(transpose(COEFS_3_square));
R=MD(COEFS_3_square,B(3,:));
RR=MD1(COEFS_3_square,C(3,:));
[P,E(3,:)]=EC(R);
[PP,EE(3,:)]=EC1(RR);
%---------------------------------------
B(4,:) = sum(COEFS_4_square);
C(4,:)= sum(transpose(COEFS_4_square));
R=MD(COEFS_4_square,B(4,:));
RR=MD1(COEFS_4_square,C(4,:));
[P,E(4,:)]=EC(R);
[PP,EE(4,:)]=EC1(RR);
%---------------------------------------
B(5,:) = sum(COEFS_5_square);
C(5,:)= sum(transpose(COEFS_5_square));
R=MD(COEFS_5_square,B(5,:));
RR=MD1(COEFS_5_square,C(5,:));
[P,E(5,:)]=EC(R);
[PP,EE(5,:)]=EC1(RR);
%---------------------------------------
B(6,:) = sum(COEFS_6_square);
C(6,:)= sum(transpose(COEFS_6_square));
R=MD(COEFS_6_square,B(6,:));
RR=MD1(COEFS_6_square,C(6,:));
[P,E(6,:)]=EC(R);
[PP,EE(6,:)]=EC1(RR);
%---------------------------------------
B(7,:) = sum(COEFS_7_square);
C(7,:)= sum(transpose(COEFS_7_square));
R=MD(COEFS_7_square,B(7,:));
RR=MD1(COEFS_7_square,C(7,:));
[P,E(7,:)]=EC(R);
[PP,EE(7,:)]=EC1(RR);
%---------------------------------------
B(8,:) = sum(COEFS_8_square);
C(8,:)= sum(transpose(COEFS_8_square));
```

```
R=MD(COEFS_8_square,B(8,:));
RR=MD1(COEFS_8_square,C(8,:));
[P,E(8,:)]=EC(R);
[PP,EE(8,:)]=EC1(RR);
%---------------------------------------
B(9,:) = sum(COEFS_9_square);
C(9,:)= sum(transpose(COEFS_9_square));
R=MD(COEFS_9_square,B(9,:));
RR=MD1(COEFS_9_square,C(9,:));
[P,E(9,:)]=EC(R);
[PP,EE(9,:)]=EC1(RR);
%---------------------------------------
B(10,:) = sum(COEFS_10_square);
C(10,:)= sum(transpose(COEFS_10_square));
R=MD(COEFS_10_square,B(10,:));
RR=MD1(COEFS_10_square,C(10,:));
[P,E(10,:)]=EC(R);
[PP,EE(10,:)]=EC1(RR);
%---------------------------------------
B(11,:) = sum(COEFS_11_square);
C(11,:)= sum(transpose(COEFS_11_square));
R=MD(COEFS_11_square,B(11,:));
RR=MD1(COEFS_11_square,C(11,:));
[P,E(11,:)]=EC(R);
[PP,EE(11,:)]=EC1(RR);
%---------------------------------------
B(12,:) = sum(COEFS_12_square);
C(12,:)= sum(transpose(COEFS_12_square));
R=MD(COEFS_12_square,B(12,:));
RR=MD1(COEFS_12_square,C(12,:));
[P,E(12,:)]=EC(R);
[PP,EE(12,:)]=EC1(RR);
%---------------------------------------
B(13,:) = sum(COEFS_13_square);
C(13,:)= sum(transpose(COEFS_13_square));
R=MD(COEFS_13_square,B(13,:));
RR=MD1(COEFS_13_square,C(13,:));
[P,E(13,:)]=EC(R);
[PP,EE(13,:)]=EC1(RR);
%---------------------------------------
B(14,:) = sum(COEFS_14_square);
C(14,:)= sum(transpose(COEFS_14_square));
R=MD(COEFS_14_square,B(14,:));
RR=MD1(COEFS_14_square,C(14,:));
[P,E(14,:)]=EC(R);
[PP,EE(14,:)]=EC1(RR);

M(1,1)=mean(E(1,:));
M(2,1)=mean(E(2,:));
M(3,1)=mean(E(3,:));
M(4,1)=mean(E(4,:));
M(5,1)=mean(E(5,:));
```

```
M(6,1)=mean(E(6,:));
M(7,1)=mean(E(7,:));
M(8,1)=mean(E(8,:));
M(9,1)=mean(E(9,:));
M(10,1)=mean(E(10,:));
M(11,1)=mean(E(11,:));
M(12,1)=mean(E(12,:));
M(13,1)=mean(E(13,:));
M(14,1)=mean(E(14,:))

MM(1,1)=mean(EE(1,:));
MM(2,1)=mean(EE(2,:));
MM(3,1)=mean(EE(3,:));
MM(4,1)=mean(EE(4,:));
MM(5,1)=mean(EE(5,:));
MM(6,1)=mean(EE(6,:));
MM(7,1)=mean(EE(7,:));
MM(8,1)=mean(EE(8,:));
MM(9,1)=mean(EE(9,:));
MM(10,1)=mean(EE(10,:));
MM(11,1)=mean(EE(11,:));
MM(12,1)=mean(EE(12,:));
MM(13,1)=mean(EE(13,:));
MM(14,1)=mean(EE(14,:))
Mean_of_coefs_1= mean(B(1,:));

figure
plot(1:14,MM,'r');
hold on
plot(1:14,M,'k');


FREQUENCY=10:200;

figure

plot(FREQUENCY,C(1,:),'*r');

S(1,1)=std(E(1,:));
S(2,1)=std(E(2,:));
S(3,1)=std(E(3,:));
S(4,1)=std(E(4,:));
S(5,1)=std(E(5,:));
S(6,1)=std(E(6,:));
S(7,1)=std(E(7,:));
S(8,1)=std(E(8,:));
S(9,1)=std(E(9,:));
S(10,1)=std(E(10,:));
S(11,1)=std(E(11,:));
S(12,1)=std(E(12,:));
S(13,1)=std(E(13,:));
```

```
S(14,1)=std(E(14,:))

SS(1,1)=std(EE(1,:));
SS(2,1)=std(EE(2,:));
SS(3,1)=std(EE(3,:));
SS(4,1)=std(EE(4,:));
SS(5,1)=std(EE(5,:));
SS(6,1)=std(EE(6,:));
SS(7,1)=std(EE(7,:));
SS(8,1)=std(EE(8,:));
SS(9,1)=std(EE(9,:));
SS(10,1)=std(EE(10,:));
SS(11,1)=std(EE(11,:));
SS(12,1)=std(EE(12,:));
SS(13,1)=std(EE(13,:));
SS(14,1)=std(EE(14,:))
```

2. Function MD

```
% probability calculation
function [M]=MD(CS, HK)

[x,y] = size(CS);
   for i=1:x


      for j=1:y
      M(i,j)= CS(i,j)/(HK(1,j));
      end
   end

end
```

3. Function MD1

```
% probability calculation
function [M]=MD1(CS, HK)

[x,y] = size(CS);
   for i=1:x
```

```
    for j=1:y
    M(i,j)= CS(i,j)/(HK(1,i));

    end
  end

end
```

4. Function EC

```
% Entropy calculation
function [M,E]=EC(P)

[x,y] = size(P);
  for i=1:x


    for j=1:y
    M(i,j)= P(i,j)*log(P(i,j));

    end
  end

  E=-sum(M);
  for k=1:2000
   TF = isnan(E(1,k));
    if(TF==1)
       E(1,k)=0;
    end
  end

end
```

5. Function EC1

```
% Entropy calculation
function [M,E]=EC1(P)

[x,y] = size(P);
  for i=1:x
```

```
    for j=1:y
    M(i,j)= P(i,j)*log(P(i,j));

    end
  end
  E=-sum(M');
  for k=1:length(E)
   TF = isnan(E(1,k));
    if(TF==1)
       E(1,k)=0;
    end
  end


end
```

Section Two: Mathematical derivation of Wavelets

The following two integrals are fundamentally implemented in mathematical derivation of wavelets

1.

$$\int_0^\infty x^n\, e^{-ax^2} dx = \begin{Bmatrix} \frac{1}{2}\Gamma\left(\frac{n+1}{2}\right) \Big/ a^{\frac{n+1}{2}} & (n > -1, a > 0) \\ \frac{(2k-1)!!}{2^{k+1}a^k}\sqrt{\frac{\pi}{a}} & (n = 2k, k\ integer, a > 0) \\ \frac{k!}{2a^{k+1}} & (n = 2k+1, k\ integer, a > 0) \end{Bmatrix}$$

$$!! = double\ factorial$$

2.

$$\int_{-\infty}^{\infty} e^{-ax^2} e^{-2bx} = \sqrt{\frac{\pi}{a}} e^{\frac{b^2}{a}}\ (a > 0)$$

$$\int_{-\infty}^{\infty} e^{-ax^2} = \sqrt{\frac{\pi}{a}} (a > 0)$$

1. Mexican hat

1.1. Fourier Transform

Mexican hat is the negative normalized second derivative order of Gaussian function

Gaussian function:

$$g(t) = e^{\frac{-t^2}{2}}$$

$$g(\omega) = \int_{-\infty}^{\infty} e^{\frac{-t^2}{2}} e^{-j\omega t}\, dt$$

$$g(\omega) = \int_{-\infty}^{\infty} e^{\frac{-t^2}{2} - j\omega t}\, dt$$

Completing the square:

$$g(\omega) = \int_{-\infty}^{\infty} e^{\frac{-(t^2+2j\omega t+\omega^2-\omega^2)}{2}}\, dt$$

$$g(\omega) = e^{\frac{-\omega^2}{2}} \int_{-\infty}^{\infty} e^{\frac{-(t^2+2j\omega t-\omega^2)}{2}}$$

$$k = t + j\omega$$

$$k^2 = (t + j\omega)^2 = t^2 + 2j\omega t - \omega^2$$

$$g(\omega) = e^{\frac{-\omega^2}{2}} \int_{-\infty}^{\infty} e^{\frac{-k^2}{2}}$$

$$\int_{-\infty}^{\infty} e^{\frac{-k^2}{2}} = \sqrt{2\pi}$$

Fourier Transform of Gaussian function:

$$g(\omega) = \sqrt{2\pi}\, e^{\frac{-\omega^2}{2}}$$

Properties of Fourier Transform:

$$\mathcal{F}[\frac{d^n g}{dt^n}] = (j\omega)^n g(\omega)$$

Therefore, the second derivative of Gaussian is:

$$\mathcal{F}[\frac{d^2 g}{dt^2}] = (j\omega)^2 g(\omega) = -\sqrt{2\pi}\,\omega^2 e^{\frac{-\omega^2}{2}}$$

$$Mexican\ hat = -\sqrt{2\pi}\,\omega^2 e^{\frac{-\omega^2}{2}}$$

Negative sign is removed because Mexican hat is negative second derivative order of Gaussian

1.2. Normalization factor

$$\psi(\mathrm{t}) = \sqrt{1/E}(1-\mathrm{t}^2)\mathrm{e}^{\frac{-\mathrm{t}^2}{2}}$$

$$\mathrm{E} = \int_{-\infty}^{\infty} |(1-\mathrm{t}^2)\mathrm{e}^{\frac{-\mathrm{t}^2}{2}}|^2 = \int_{-\infty}^{\infty} (1-2\mathrm{t}^2+\mathrm{t}^4)\,\mathrm{e}^{-\mathrm{t}^2}$$

$$E = \int_{-\infty}^{\infty} e^{-t^2} + \int_{-\infty}^{\infty} -2t^2\, e^{-t^2} + \int_{-\infty}^{\infty} t^4\, e^{-t^2}$$

$$\int_{-\infty}^{\infty} e^{-t^2} = \sqrt{\pi}$$

$$\int_{-\infty}^{\infty} -2t^2\, e^{-t^2} = \frac{-2}{2}\sqrt{\frac{\pi}{1}} = -\sqrt{\pi}$$

$$\int_{-\infty}^{\infty} t^4\, e^{-t^2} = \frac{2 * 3!!}{2^3 1^2}\sqrt{\frac{\pi}{1}} = \frac{3}{4}\sqrt{\pi}$$

$$E = \sqrt{\pi} - \sqrt{\pi} + \frac{3}{4}\sqrt{\pi} = \frac{3}{4}\sqrt{\pi}$$

$$\psi(t) = \frac{1}{\sqrt{E}}(1 - t^2)e^{\frac{-t^2}{2}} = \frac{2}{\sqrt{3}\sqrt[4]{\pi}}(1 - t^2)e^{\frac{-t^2}{2}}$$

1.3. Admissibility constant

$$C_g = \int_0^{\infty} \frac{|\psi(f)|^2}{f}\, df < \infty$$

$$|\psi(f)|^2 = 32\pi^5 f^4 e^{-4\pi^2 f^2}$$

$$C_g = \int_0^{\infty} \frac{32\pi^5 f^4 e^{-4\pi^2 f^2}}{f}\, df < \infty$$

$$C_g = \int_0^{\infty} 32\pi^5 f^3 e^{-4\pi^2 f^2}\ df < \infty$$

$$C_g = \frac{32\pi^5}{2(4\pi)^2} = \pi$$

1.4. Central frequency of Mexican hat

$$f_c = \sqrt{\frac{\int_0^{\infty} f^2 |\psi(f)|^2}{\int_0^{\infty} |\psi(f)|^2}}$$

From integrals fundamentals (1)

$$\int_0^{\infty} |\psi(f)|^2 = \int_0^{\infty} 32\pi^5 f^4 e^{-4\pi^2 f^2} = 32\pi^5 \frac{3!!}{2^3(4\pi^2)^2}\sqrt{\frac{\pi}{4\pi^2}}$$

$$\int_0^{\infty} f^2 |\psi(f)|^2 = \int_0^{\infty} f^2 * 32\pi^5 f^4 e^{-4\pi^2 f^2} = \int_0^{\infty} 32\pi^5 f^6 e^{-4\pi^2 f^2} = 32\pi^5 \frac{5!!}{2^4(4\pi^2)^3}\sqrt{\frac{\pi}{4\pi^2}}$$

$$f_c = \sqrt{\frac{32\pi^5 \frac{5!!}{2^4(4\pi^2)^3}\sqrt{\frac{\pi}{4\pi^2}}}{32\pi^5 \frac{3!!}{2^3(4\pi^2)^2}\sqrt{\frac{\pi}{4\pi^2}}}} = {\sqrt{(5/2)}}/{2\pi} \approx 0.251$$

2. Complex Morlet

1.5. Fourier Transform

$$g(f) = \int_{-\infty}^{\infty} e^{2i\pi f_c t} e^{\frac{-t^2}{f_b}} e^{-2i\pi f t}\, dt$$

$$g(f) = \int_{-\infty}^{\infty} e^{\frac{-t^2}{f_b}} e^{-2i\pi (f-f_c) t}\, dt$$

$$b = i\pi(f - f_c)$$

$$b^2 = -(\pi f - \pi f_c)^2$$

$$a = \frac{1}{f_b}$$

$$g(f) = \sqrt{\pi f_b}\, e^{-f_b(\pi f - \pi f_c)^2}$$

Rewritten as

$$g(f) = \sqrt{\pi f_b} e^{\frac{-f_b}{4}(2\pi f - 2\pi f_c)^2}$$

1.6. Normalization factor

A. The normalization factor is derived based on first dimension of Hilbert space, L,

$$\psi(t) = \frac{1}{E} e^{2i\pi f_c t} e^{\frac{-t^2}{f_b}} \quad 1$$

$$E = \int_{-\infty}^{\infty} e^{2i\pi f_c t} e^{\frac{-t^2}{f_b}}$$

$$e^{2i\pi f_c t} = (\cos 2i\pi f_c t + i \sin 2i\pi f_c t)$$

$$|(\cos 2i\pi f_c t + i \sin 2i\pi f_c t)| = 1$$

$$E = \int_{-\infty}^{\infty} e^{\frac{-t^2}{f_b}}$$

$$E = \sqrt{\pi f_b}$$

B. The normalization factor is derived based on $2^{nd} - norm$ in Hilbert space,L^2

$$\psi(t) = \frac{1}{\sqrt{E}} e^{2i\pi f_c t} e^{\frac{-t^2}{f_b}} \qquad (\mathbf{1})$$

$$E = \int_{-\infty}^{\infty} \left| (e^{2i\pi f_c t} e^{\frac{-t^2}{f_b}}) \right|^2 = \int_{-\infty}^{\infty} |(\cos 2i\pi f_c t + i \sin 2i\pi f_c t)|^2 e^{\frac{-2t^2}{f_b}} \qquad (\mathbf{2})$$

$$|(\cos 2i\pi f_c t + i \sin 2i\pi f_c t)| = 1$$

$$E = \int_{-\infty}^{\infty} 1 * e^{\frac{-2t^2}{f_b}} = \sqrt{\frac{\pi f_b}{2}} \qquad (\mathbf{3})$$

From 1 and 3

$$\psi(t) = \frac{1}{\sqrt{\sqrt{\frac{\pi f_b}{2}}}} e^{2i\pi f_c t} e^{\frac{-t^2}{f_b}}$$

$$\psi(t) = \frac{1}{\sqrt[4]{\frac{\pi f_b}{2}}} e^{2i\pi f_c t} e^{\frac{-t^2}{f_b}}$$

3. Complex Shannon Wavelet

1.1. Normalization factor

The normalization factor is derived based on $2^{\mathrm{nd}} - \mathrm{norm}$ in Hilbert space, L^2

$$\psi(t) = \frac{1}{\sqrt{E}}\mathrm{sinc}(f_b t)e^{2i\pi f_c t} \qquad (\mathbf{1})$$

$$E = \int_{-\infty}^{\infty}(\mathrm{sinc}(f_b t)e^{2i\pi f_c t})^2 \qquad (\mathbf{2})$$

$$e^{2i\pi f_c t} = (\cos 2i\pi f_c t + i \sin 2i\pi f_c t)$$

$$|(\cos 2i\pi f_c t + i \sin 2i\pi f_c t)| = 1$$

Therefore

$$E = \int_{-\infty}^{\infty}(\mathrm{sinc}(f_b t))^2 \, dt$$

$$x = f_b t$$

$$dx = f_b \, dt$$

$$E = \int_{-\infty}^{\infty}(\mathrm{sinc}(x))^2 \frac{dx}{f_b}$$

$$\int_{-\infty}^{\infty}(\mathrm{sinc}(x))^2 = 1$$

$$\mathrm{E} = \frac{1}{\mathrm{f_b}} \qquad (\mathbf{3})$$

From 1 and 3, the normalized complex Shannon wavelet, therefore:

$$\psi(\mathrm{t}) = \sqrt{\mathrm{f_b}}\mathrm{sinc}(\mathrm{f_b t})\mathrm{e}^{2\mathrm{i}\pi \mathrm{f_c t}}$$

4. The Gabor Transform

4.1. Normalization factor

The normalization factor is derived based on $2^{\mathrm{nd}} - \mathrm{norm}$ in Hilbert space, L^2

$$h(t) = \frac{1}{\sqrt{E}} e^{\frac{-1}{2}(t^2/\sigma^2)}$$

$$\mathrm{E} = \int_{-\infty}^{\infty} (e^{\frac{-1}{2}(t^2/\sigma^2)})^2$$

$$\mathrm{E} = \int_{-\infty}^{\infty} e^{-(t^2/\sigma^2)} = \sigma\sqrt{\pi}$$

$$h(t) = \frac{1}{\sqrt{\sigma}\pi^{\frac{1}{4}}} e^{\frac{-1}{2}(t^2/\sigma^2)}$$

Section Three: Results

Wavelet Time Entropy and Wavelet Frequency Entropy

1. Biceps muscle

1.1. Complex Morlet

1.1.1. Average (Type 1)

	Wavelet Time Entropy			Wavelet Frequency Entropy		
Frequency Bandwidth	1	2	3	1	2	3
Central frequency						
0.5	4.523	4.5194	4.4695	6.7716	6.7753	6.8116
1	4.4382	4.3817	4.3611	6.8417	6.9055	6.9363
1.5	4.375	4.3439	4.3238	6.9147	6.9639	6.9888
2	4.349	4.3139	4.2852	6.956	6.9978	7.0156
2.5	4.328	4.2818	4.2489	6.9839	7.0168	7.0286
3	4.3053	4.2519	4.2181	7.0024	7.0266	7.0354
3.5	4.2828	4.2262	4.1936	7.0149	7.0333	7.041
4	4.2598	4.201	4.1714	7.0219	7.0361	7.0438
4.5	4.2386	4.1841	4.1605	7.0275	7.0409	7.05
5	4.2172	4.166	4.1466	7.0306	7.0435	7.0537
5.5	4.2039	4.1575	4.1435	7.0334	7.0476	7.0603
6	4.1815	4.1401	4.1341	7.0363	7.0514	7.0655
6.5	4.1609	4.1307	4.1324	7.0363	7.0548	7.0714
7	4.1299	4.1166	4.1281	7.0397	7.0595	7.0772

1.1.2. Standard Deviation (Type 1)

	Wavelet Time Entropy			Wavelet Frequency Entropy		
Frequency Bandwidth	1	2	3	1	2	3
Central frequency						
0.5	0.451	0.3276	0.3044	0.1324	0.1509	0.1416
1	0.2887	0.2603	0.2497	0.1309	0.1119	0.1085
1.5	0.2564	0.2426	0.2359	0.1102	0.1073	0.1068
2	0.2442	0.2323	0.2259	0.1072	0.1063	0.1071
2.5	0.2366	0.2255	0.2221	0.1063	0.1072	0.1114
3	0.2307	0.2227	0.2261	0.105	0.1092	0.1151
3.5	0.2264	0.2251	0.2367	0.1053	0.1129	0.12
4	0.2246	0.2357	0.2545	0.105	0.1134	0.1224
4.5	0.2299	0.2471	0.2682	0.1084	0.1197	0.1306
5	0.2391	0.2664	0.2924	0.11	0.1234	0.1352
5.5	0.2427	0.2776	0.3046	0.1119	0.1281	0.1408
6	0.2731	0.319	0.3412	0.1143	0.1319	0.1442
6.5	0.2882	0.3347	0.3525	0.1145	0.1332	0.1455
7	0.3386	0.3676	0.3732	0.1195	0.1395	0.1516

1.1.3. Average (Type 2)

	Wavelet Time Entropy			Wavelet Frequency Entropy		
Central frequency	1	2	3	1	2	3
Frequency Bandwidth						
0.5	4.5151	4.3813	4.3428	6.7764	6.9053	6.9625
1	4.4382	4.349	4.3053	6.8417	6.956	7.0024
1.5	4.4017	4.3304	4.2753	6.8811	6.9818	7.0184
2	4.3817	4.3139	4.2519	6.9055	6.9978	7.0266
2.5	4.3696	4.2988	4.2332	6.9229	7.0083	7.0317
3	4.3611	4.2852	4.2181	6.9363	7.0156	7.0354
3.5	4.3546	4.273	4.2057	6.9471	7.0208	7.0383
4	4.349	4.2622	4.1955	6.9563	7.0248	7.0408
4.5	4.3439	4.2525	4.187	6.9641	7.028	7.043
5	4.3392	4.2436	4.1798	6.9709	7.0305	7.0451
5.5	4.3346	4.2356	4.1738	6.9769	7.0326	7.0471
6	4.3303	4.2283	4.1686	6.9821	7.0345	7.049
6.5	4.326	4.2216	4.1642	6.9868	7.0361	7.0509
7	4.3219	4.2155	4.1605	6.991	7.0375	7.0528

1.1.4. Standard Deviation (Type 2)

	Wavelet Time Entropy			Wavelet Frequency Entropy		
Central frequency	1	2	3	1	2	3
Frequency Bandwidth						
0.5	0.3313	0.2643	0.2422	0.1501		0.1056
1	0.2887	0.2426	0.2307	0.1309	0.1309	0.105
1.5	0.2706	0.2294	0.2251	0.1177	0.1335	0.1064
2	0.2603	0.2196	0.2227	0.1119	0.1284	0.1092
2.5	0.2539	0.2125	0.2234	0.1095	0.1207	0.1122
3	0.2497	0.2074	0.2261	0.1085	0.1138	0.1151
3.5	0.2468	0.2037	0.2299	0.108	0.1081	0.1178
4	0.2446	0.2008	0.2343	0.1076	0.1038	0.1204
4.5	0.2427	0.1983	0.2391	0.1073	0.1007	0.1229
5	0.241	0.196	0.2441	0.1071	0.0988	0.1254
5.5	0.2394	0.1937	0.2491	0.107	0.0978	0.1278
6	0.2379	0.1915	0.2541	0.1069	0.0975	0.1302
6.5	0.2364	0.1892	0.259	0.1068	0.0976	0.1324
7	0.2351	0.1869	0.2639	0.1067	0.0981	0.1346

1.2. Complex Shannon

1.2.1. Average (Type 1)

	Wavelet Time Entropy			Wavelet Frequency Entropy		
Frequency Bandwidth	1	2	3	1	2	3
Central frequency						
0.5	4.2556	4.0582	4.2301	6.643	6.6198	6.649
1	4.0369	4.255	4.0576	6.8168	6.642	6.6264
1.5	4.1108	3.9451	4.2557	6.8583	6.7821	6.6415
2	4.1495	4.0139	3.9247	6.8939	6.8128	6.7495
2.5	4.1771	4.0561	3.954	6.9242	6.8347	6.7951
3	4.1597	4.0788	3.9983	6.9449	6.8528	6.8093
3.5	3.9862	3.8343	3.6706	6.9374	6.8404	6.7925
4	3.5958	3.332	3.0235	6.8881	6.7746	6.6994
4.5	3.0902	2.8138	2.6137	6.8212	6.6985	6.547
5	2.6018	2.9269	3.7083	6.7599	6.5845	6.4562
5.5	3.0374	3.5643	2.5777	6.6791	6.469	6.5914
6	3.324	2.6426	2.7913	6.5016	6.6433	6.6546
6.5	3.3292	2.4735	2.8386	6.658	6.6823	6.6923
7	3.545	3.4652	2.5582	6.5395	6.5449	6.6396

1.2.2. Standard Deviation (Type 1)

	Wavelet Time Entropy			Wavelet Frequency Entropy		
Frequency Bandwidth	1	2	3	1	2	3
Central frequency						
0.5	0.5448	0.6933	0.5453	0.1133	0.0988	0.0917
1	0.2893	0.5453	0.6907	0.0772	0.1125	0.1053
1.5	0.2635	0.3205	0.5471	0.097	0.0708	0.1122
2	0.248	0.289	0.3222	0.0963	0.0773	0.0727
2.5	0.2189	0.2684	0.3105	0.0946	0.0892	0.065
3	0.2417	0.2678	0.2854	0.0945	0.0942	0.0746
3.5	0.2353	0.2647	0.2844	0.0945	0.0889	0.0803
4	0.2263	0.2614	0.3401	0.1097	0.1182	0.121
4.5	0.2643	0.3196	0.5144	0.1423	0.1305	0.1395
5	0.3171	0.5413	0.2391	0.1263	0.1411	0.0894
5.5	0.5071	0.2784	0.4204	0.1133	0.101	0.1364
6	0.3745	0.5104	0.3285	0.1155	0.1248	0.14
6.5	0.5447	0.405	0.325	0.1112	0.1277	0.128

7	0.3331	0.5475	0.4022		0.1286	0.1228	0.121

1.2.3. Average (Type 2)

	Wavelet Time Entropy				Wavelet Frequency Entropy		
Central frequency	1	2	3		1	2	3
Frequency Bandwidth							
0.5	4.1718	4.2166	4.2866		6.8975	6.9789	7.0222
1	4.0369	4.1495	4.1597		6.8168	6.8939	6.9449
1.5	3.9668	4.0807	4.1249		6.7545	6.843	6.8906
2	4.255	4.0139	4.0788		6.642	6.8128	6.8528
2.5	4.0248	3.9489	4.0473		6.6384	6.793	6.8245
3	4.0576	3.9247	3.9983		6.6264	6.7495	6.8093
3.5	4.1538	4.0007	3.951		6.6322	6.7358	6.7958
4	4.2384	4.2556	3.9245		6.6641	6.6412	6.7761
4.5	4.2933	4.0247	3.9134		6.6725	6.6389	6.7462
5	4.338	4.0552	3.9546		6.6857	6.6296	6.7309
5.5	4.3752	4.1522	4.0004		6.7004	6.6395	6.7343
6	4.4006	4.241	4.2531		6.7062	6.6751	6.6415
6.5	4.4117	4.2713	4.1285		6.7062	6.6772	6.5782
7	4.3791	4.1799	4.0538		6.6917	6.639	6.5777

1.2.4. Standard Deviation (Type 2)

	Wavelet Time Entropy			Wavelet Frequency Entropy		
Central frequency	1	2	3	1	2	3
Frequency Bandwidth						
0.5	0.2468	0.2143	0.2244	0.0978	0.1042	0.0999
1	0.2893	0.248	0.2417	0.0772	0.0963	0.0945
1.5	0.3211	0.2635	0.2495	0.0669	0.0931	0.0931
2	0.5453	0.289	0.2678	0.1125	0.0773	0.0942
2.5	0.7093	0.3136	0.2621	0.0706	0.0673	0.0908
3	0.6907	0.3222	0.2854	0.1053	0.0727	0.0746
3.5	0.6163	0.3016	0.3029	0.1096	0.0736	0.0692
4	0.5481	0.5475	0.3189	0.0858	0.1121	0.0687
4.5	0.4994	0.7095	0.3233	0.0911	0.0716	0.0742
5	0.4606	0.6901	0.3073	0.0949	0.1074	0.0745
5.5	0.429	0.6145	0.2965	0.0897	0.1135	0.0806
6	0.4089	0.5471	0.5458	0.0929	0.0903	0.1124
6.5	0.3983	0.5194	0.5192	0.0922	0.0966	0.0613
7	0.4243	0.5756	0.595	0.0821	0.0923	0.067

1.3. Derivative of Gaussian and Derivative of Complex Gaussian

1.3.1. Average

	Derivative of Complex Gaussian		Derivative of Gaussian	
	Wavelet Time Entropy	Wavelet Frequency Entropy	Wavelet Time Entropy	Wavelet Frequency Entropy
Order				
1	4.6452	6.6877	4.4628	6.445
2	4.5616	6.7155	4.3639	6.416
3	4.5632	6.7633	4.3528	6.4552
4	4.4389	6.773	4.3863	6.4771
5	4.49	6.8042	4.2586	6.4844
6	4.4084	6.8144	4.3267	6.5092
7	4.4688	6.836	4.2317	6.516
8	4.4087	6.8441	4.1783	6.5244

1.3.2. Standard Deviation

	Derivative of Complex Gaussian		Derivative of Gaussian	
	Wavelet Time Entropy	Wavelet Frequency Entropy	Wavelet Time Entropy	Wavelet Frequency Entropy
Order				
1	0.3794	0.1425	0.5172	0.0948
2	0.356	0.1553	0.4677	0.136
3	0.3329	0.1536	0.4493	0.1445
4	0.3234	0.1404	0.3931	0.1546
5	0.3105	0.1427	0.4157	0.1415
6	0.3039	0.1321	0.3659	0.1456
7	0.2929	0.1342	0.3847	0.1359
8	0.2892	0.1263	0.359	0.1272

1.4. Symlets , Coiflets and Daubechies

1.4.1. Average

	Symlets		Coiflets		Daubechies	
	Wavelet Time Entropy	Wavelet Frequency Entropy	Wavelet Time Entropy	Wavelet Frequency Entropy	Wavelet Time Entropy	Wavelet Frequency Entropy
Order						
1	4.598	6.4484	4.4268	6.4311	4.598	6.4484
2	4.3289	6.4325	4.3304	6.4507	4.3289	6.4325
3	4.4041	6.47	4.2925	6.4702	4.4041	6.47
4	4.3064	6.4404	4.2698	6.4838	4.2996	6.489
5	4.258	6.4509	4.256	6.4936	4.2224	6.5058
6	4.312	6.4674			4.2763	6.5322
7	4.2488	6.4765			4.2284	6.5451
8	4.2372	6.4773			4.1872	6.557
9	4.2713	6.4811			4.2169	6.5717
10	4.2499	6.4929			4.1799	6.5791
11	4.1915	6.4901			4.1511	6.5858
12	4.2467	6.4934			4.1823	6.5944
13	4.2134	6.4953			4.1537	6.5991
14	4.2149	6.4968			4.1267	6.6035
15	4.2063	6.5034			4.1509	6.6095

1.4.2. Standard Deviation

	Symlets		Coiflets		Daubechies	
	Wavelet Time Entropy	Wavelet Frequency Entropy	Wavelet Time Entropy	Wavelet Frequency Entropy	Wavelet Time Entropy	Wavelet Frequency Entropy
Order						
1	0.486	0.4838	0.4737	0.1478	0.486	0.4838
2	0.4798	0.1173	0.4232	0.1395	0.4798	0.1173
3	0.4185	0.145	0.3979	0.134	0.4185	0.145
4	0.4371	0.1401	0.3836	0.1306	0.402	0.13
5	0.4102	0.128	0.3767	0.1283	0.3962	0.1204
6	0.402	0.1393		.	0.37	0.1247
7	0.4114	0.1269			0.3538	0.1175
8	0.3879	0.128			0.3346	0.1109
9	0.3851	0.1324			0.3274	0.1128
10	0.3799	0.1282			0.3329	0.1072
11	0.3896	0.1215			0.3274	0.1025
12	0.361	0.1287			0.3089	0.1039
13	0.3888	0.1273			0.3055	0.0997
14	0.363	0.1239			0.3053	0.0962
15	0.37	0.1242			0.3007	0.0976

2. Flexor Digitorum Superficial muscle

2.1. 15% Force Contraction

	WTE	WFE
wavelet		
Complex Morlet (7,3)	2.9515	6.4477
Complex Morlet (2,1)	3.3997	4.8942
Complex Shannon (1,5)	1.1059	5.6467
Complex Shannon (2,1.5)	3.1483	4.5523
Gaussian-8	3.3696	4.5412
Daubechie-14	3.2807	4.9381
Symlets-14	3.4499	4.4625

2.2. 50% Force Contraction

	WTE	WFE
wavelet		
Complex Morlet (3,7)	3.1081	6.064
Complex Morlet (3,1)	3.3376	4.5859
Complex Shannon (2,4.5)	1.4772	5.2093
Complex Shannon (2,1.5)	3.1583	4.0056
Gaussian-8	3.3483	4.1691
Daubechie-14	3.2225	4.5955
Symlet-14	3.4523	4.0909

2.3. 70% Force Contraction

	WTE	WFE
wavelet		
Complex Morlet (7,3)	3.2078	6.2716
Complex Morlet (2,1)	3.3826	5.3416
Complex Shannon (1,4.5)	1.4415	6.2788
Complex Shannon (0.5,1)	3.0865	5.9062
Gaussian-8	3.2204	4.9822
Daubechie-14	3.1497	5.1089
symlet-14	3.2928	4.8314

2.4. 90% Force Contraction

	WTE	WFE
wavelet		
Complex Morlet (3,6)	3.3122	6.0161
Complex Morlet (2,1)	3.4966	4.5981
Complex Shannon (2,4.5)	1.259	5.4707
Complex Shannon (2,1.5)	3.1397	4.0576
Gaussian-8	3.3764	4.2357
Daubechie-14	3.2808	4.529
symlet-14	3.4367	4.1364

Section Four: Central Frequencies

1. Symlets , Coiflets and Daubechies

	Symlets	Coiflets	Daubechies
Order			
1	0.9961	0.8	0.9961
2	0.6667	0.7273	0.6667
3	0.8	0.7059	0.8
4	0.7143	0.6957	0.7143
5	0.6667	0.6897	0.6667
6	0.7273		0.7273
7	0.6923		0.6923
8	0.6667		0.6667
9	0.7059		0.7059
10	0.6842		0.6842
11	0.6667		0.6667
12	0.6957		0.6957
13	0.68		0.68
14	0.6667		0.6667
15	0.6897		0.6897

2. DOG , DOCG , Mexican hat and Meyer

	DOG	DOCG
Derivative		
1	0.2	0.3
2	0.3	0.4
3	0.4	0.5
4	0.5	0.5
5	0.5	0.6
6	0.6	0.6
7	0.6	0.7
8	0.6	0.7

Mexican hat wavelet: 0251, Meyer wavelet: 0.6902